NASA TECHNICAL MEMORANDUM

NASA TM-77395

N84-19471

FLOW PROCESSES IN OVEREXPANDED CHEMICAL ROCKET NOZZLES. PART 2: SIDE LOADS DUE TO ASYMMETRIC SEPARATION.

Robert H. Schmucker

Translation of "Stromungsvorgange Beim Betrieb Oberexpandierter Dosen Chemischer Raketentriebwerke. Teil 2: Seitenkrafte Durch Unsymmetrische Ablosung," Technische Universitaet, Munich (West Germany), Lehrstuhl fuer Raumfahrttechnik, Report Number TUM-LRT-TB-10, 15 September 1973, pp. 1-60.

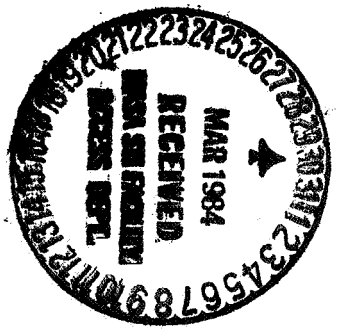

NATIONAL AERONAUTICS AND SPACE ADMINSTRATION
WASHINGTON, D.C. 20546 FEBRUARY 1984

STANDARD TITLE PAGE

1. Report No. NASA TM-77395	2. Government Accession No.	3. Recipient's Catalog No.
4. Title and Subtitle FLOW PROCESSES IN OVEREXPANDED CHEMICAL ROCKET NOZZLES. PART 2: SIDE LOADS DUE TO ASYMMETRIC SEPARATION		5. Report Date February, 1984 6. Performing Organization Code
7. Author(s) Robert H. Schmucker		8. Performing Organization Report No. 10. Work Unit No.
9. Performing Organization Name and Address SCITRAN Box 5456 Santa Barbara, CA 93108		11. Contract or Grant No. NASw 3542 13. Type of Report and Period Covered Translation
12. Sponsoring Agency Name and Address National Aeronautics and Space Administration Washington, D.C. 20546		14. Sponsoring Agency Code

15. Supplementary Notes

Translation of "Stromungsvorgange Beim Betrieb Oberexpandierter Dosen Chemischer Raketentriebwerke. Teil 2: Seitenkrafte Durch Unsymmetrische Ablosung," Technische Universitaet, Munich (West Germany), Lehrstuhl fuer Raumfahrttechnik, Report Number TUM-LRT-TB-10, 15 September 1973, pp 1-60. (N75-26012)

16. Abstract

Methods for measuring the lateral forces, occurring as a result of asymmetric nozzle flow separation, are discussed. The effect of some parameters on the side load is explained. A new method was developed for calculation of the side load. The values calculated are compared with side load data of the J-2 engine. Results are used for predicting side loads of the space shuttle main engine.

Sponsored by NASA, U.S. Academy of Sciences and Deutsche Forschungsgemeinschaft.

17. Key Words (Selected by Author(s))	18. Distribution Statement
	Unclassified and Unlimited

19. Security Classif. (of this report)	20. Security Classif. (of this page)	21. No. of Pages	22. Price
Unclassified	Unclassified	57	

FOREWORD

The investigations on "Flow Processes in Overexpanded Chemical Rocket Nozzles" were conducted from March 1972 until February 1973 within the framework of the NRC Resident Research Associateship Program of the National Academy of Sciences (USA) in the Astronautics Laboratory of the George C. Marshall Space Flight Center of NASA (NASA-MSFC), Huntsville, Alabama, USA. My gratitude for their support and encouragement is due to Mr. C.R. Bailey, Scientific Advisor, K.W. Gross, H.G. Paul, Division Chief, and D. Pryor.

Since March 1973 these investigations have been supported by the German Forschungsgemeinschaft (DEG).

The result of the work is presented in three reports from the Lehrstuhl für Raumfahrttechnik of the TUM:

Flow Processes In Overexpanded Chemical Rocket Nozzles
Part 1: Flow Separation*
Part 2: Side Forces due to Asymmetrical Separation
Part 3: Methods for Specific Flow Separation and Lateral Force Reduction.

*Translator's Note: Available in translation as NASA TM-77396.

CONTENTS

LIST OF SYMBOLS

1. Latin characters

A	surface
d	diameter
f	frequency
F	force
K	constants
l	length
M	Mach number
p	pressure
r	radius
t	time

2. Greek characters

γ	isentropic exponent
ε	surface ratio
θ	moment of inertia
Θ	jet angle
ϕ	flow angle
ψ	turning angle

3. Indices

a	flow
a	environment
ac	operating cylinder
c	combustion chamber
cg	center of mass
e	end of jet
eff	effective (RMS)
en	engine
ff	full flowing nozzles
fl	fluctuation
fs	flow separation
g	form of the separation symmetry

h	horizontal
i	start of separation
n	jet
ot	lateral support
5	re-application
sc	separation distance from the nozzle
sl	side load
t	neck
ts	test value
v	vertical
w	wall

0. SUMMARY

Side loads occur during the operating phase during which the flow is separated within the nozzle as a result of back pressure. The loads could be so great that the normal operation of the rocket engine is endangered. The various methods of side load measurement are presented and their applicability is discussed. The influence of various parameters on the side force determined by the experiment are explained. Based on the methods available for the computation of side load, which have been summarized, a new procedure for the determining of side load is described. The computed values are compared with the side load data of the J-2 engines. The results are applied to the side load predictions for the main engine for the space shuttle.

1. INTRODUCTION */1

Unsymmetrical thrust components, which act on the nozzle wall as side loads, develop during the start and combustion cut-off phases of a rocket engine which is operated within the atmosphere. These type of loads could also develop with a multi-stage missile if the engine of the upper stage is ignited before the stage separation. The pressure developed by this in spite of the external vacuum in the intermediate stage can, however, have undesirable effects on the nozzle flow and lead to side loads.

These side loads are caused by unsymmetrical nozzle flow and depend on the engine thrust, the opening ratio of the nozzle, the contour of the nozzle and the pressure of the combustion chamber and the environment. They are usually unstable and their size and direction change continually. Engines, whose nozzles in spite of a large opening ratio for vacuum operation that are especially designed so that no flow separation occurs in the nozzle at sea level with full thrust, have very large side loads.

High side loads were observed during the development program of various large engines. This phenomenon was first observed with the Atlas sustainer engine. In a certain range of the combustion chamber pressure during the initial phase, side loads developed that amounted to about 20% of the full thrust of the engine [7]. In the subsequent years the side loads were measured for the engines of the first stage of the Titan III missiles, and an unsuccessful launch of a Vanguard missile is traceable to side loads [1]. The greatest side loads were observed with the J-2 engine, the engine of the second and third stages of the Saturn V missiles. During a test when the engine was operated for several seconds with reduced combustion chamber pressure, the side loads were so large that the bolts of the gimbal joint broke and the engine was

*Numbers in margin indicate pagination of foreign text.

destroyed. These unexpected side loads led to considerable difficulties during the J-2 engine development program and led to the jets being side mounted for tests at sea level [14]. /2

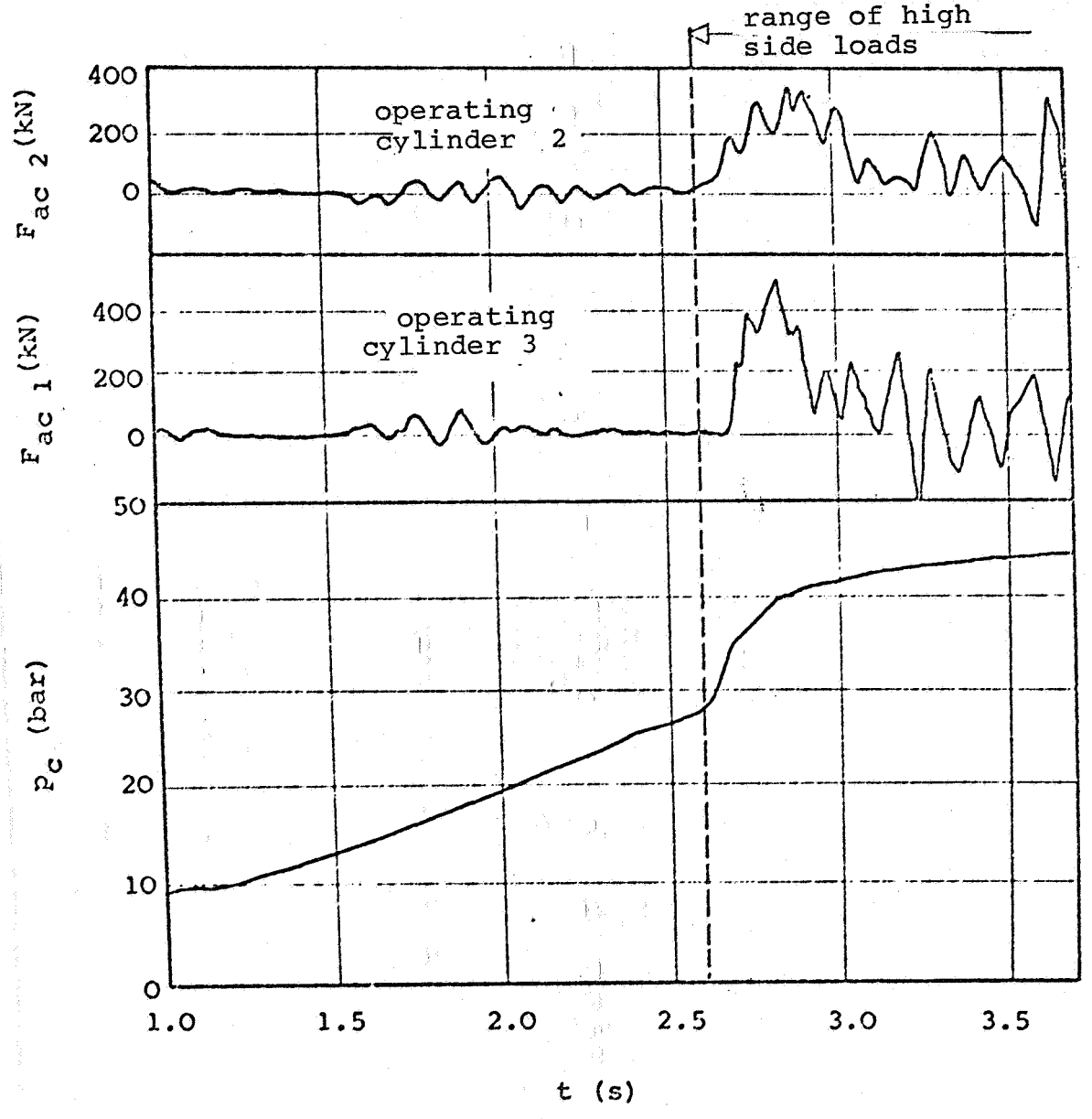

Figure 1. Load F_{ac} of the engine operating cylinder (actuator) due to side load during the initial phase of a J-2D engine (rated thrust $F = 10^6$N) [14].

High side loads must be considered as disruptions to the engine function and are of little benefit since they require a structural reinforcing of the engine and the suspension which increases the weight of the propulsion system. It is, therefore, necessary to have a quantitative understanding of the process of side load production in order to achieve small side loads in the design of the nozzles.

/3

2. PHENOMENON OF THE SIDE LOAD

In the ignition, shut-down or retardation of a rocket engine the combustion chamber pressure is lower than during full load operation. If the engine operates during this phase with back pressure, then the gas flow separates from the nozzle wall. As a result of this, side loads develop in certain areas of the combustion chamber pressure. Figure 1 shows the load F_{ac} of the engine operating cylinder due to the side loads during the initial phase of a J-2D engine. These side loads are caused by unsymmetrical separation of the jet stream in the nozzle.

/4

2.1 Unsymmetrical flow separation as a cause of the side loads

Figure 2 shows a J-2D engine during the final combustion phase of a test run. It shows the very unsymmetrical separation of the jet stream which still only fills a portion of the nozzle cross-section.

For an analysis of the effect of the unsymmetrical flow separation, it is best to consider a narrow sector of the nozzle flow in which the separation is nearly level and perpendicular to the axis.

The separation process and the wall pressure distribution with the resulting loads are shown in Figure 3. The gases expand

/5

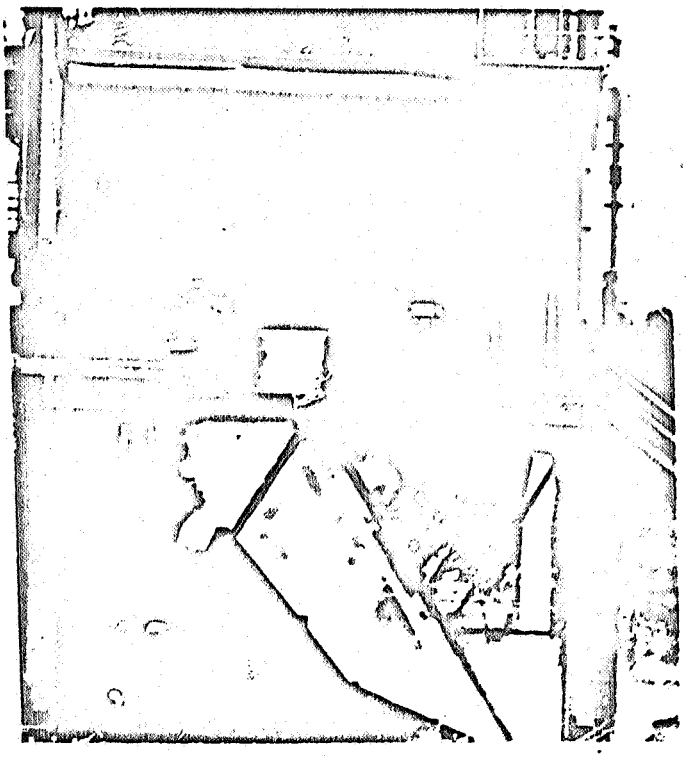

Figure 2. Unsymmetrical flow separation during the final combustion phase of a J-2D engine.

along the nozzle wall from the combustion chamber pressure p_c to the local wall pressure p_w. A boundary layer develops along the wall. Until the pressure neutral point, at which the wall pressure and the environmental pressure p_a are equal, p_w is higher than p_a, and a pressure load develops which works from inside on the nozzle wall and produces the engine thrust. As a result of the over-expansion, the wall pressure decreases below the neutral point under the environmental pressure. This produces a load which effects the nozzle wall from outside and decreases the /6
thrust. This load can lead to a considerable deformation of the nozzle wall, especially with thin-wall engines [14,20]. From a certain difference between the wall and the external pressure, the boundary layer can no longer counter the envionromental pressure, and it separates from the wall.

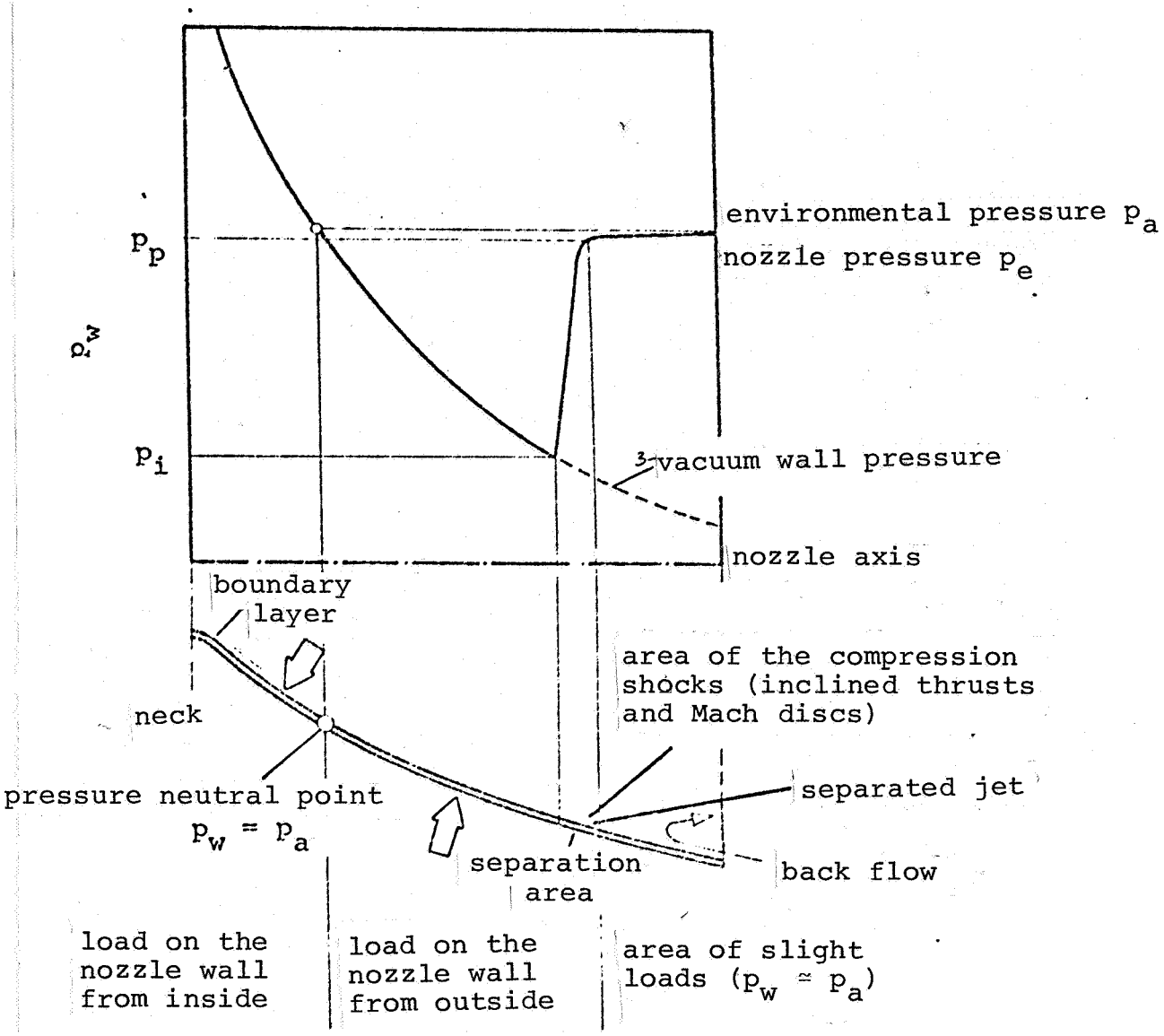

Figure 3. Flow process, pressure distribution and loads on the nozzle wall with flow separation.

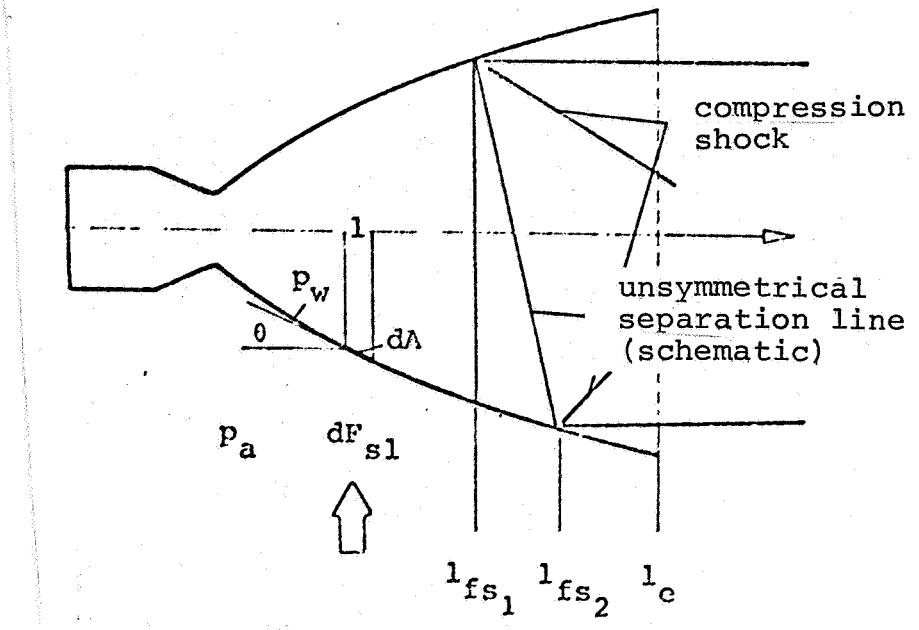

Figure 4. Unsymmetrical flow separation.

An inclined compression thrust develops which turns in the direction of the main flow. In this separation area, the wall pressure of p_i, the minimum nozzle pressure at which the separation process begins, increases within a short distance to a pressure p_p which is just slightly below the environmental pressure. Due to this slight pressure difference, the nozzle part is loaded just slightly downwards from the separation area.

The position of the pressure neutral point and the location of the separation area depend on the ratio of the combustion chamber pressure to the environmental pressure. With increasing pressure ratios, the points move toward the nozzle end.

In the case of a rotationally symmetric flow process, the pressure loads are equalized circumferentially and the thrust vector agrees with the geometric nozzle axis. If, however, the field of low and the separation line are not axially symmetric, then side loads result. Figure 4 shows the flow picture of a nozzle with unsymmetrical separation.

If the local distance of the surface element dA from the injector plate with l, then the side load F_{sl} can be written /7

$$\vec{F}_{sl} = \int_0^{l_e} \int_0^{2\pi} (p_a - p_w) \cos\theta \, d\vec{A} \qquad (1)$$

whereby θ indicates the angle of the nozzle wall. The side load according to equation (1) works perpendicularly to the nozzle axis since all axial portions are attributed to the thrust . The unsymmetrical thrust components in the direction of the nozzle axis are usually very small.

The side load equation (1) can be broken down into three terms+

$$\vec{F}_{sl} = -\int_0^{l_{fs_1}} \int_0^{2\pi} p_w \cos\theta \, d\vec{A} \qquad (2)$$

$$+\int_{l_{fs_1}}^{l_{fs_2}} \int_0^{2\pi} (p_a - p_w)\cos\theta \, d\vec{A}$$

$$-\int_{l_{fs_2}}^{l_e} \int_0^{2\pi} p_w \cos\theta \, d\vec{A}$$

The first term represents the side loads which develop in the full flowing portion of the nozzle due to an unsymmetrical pressure distribution. These side loads correspond somewhat to those of a nozzle that has not separated in full load operation. In a well formed nozzle, these loads are usually very small and their portion of the entire side load is very slight (in the J-2D engine the side loads at full thrust are <1% of the total thrust).

+Since the external pressure is considered symmetric, P_a can be partially omitted in (2).

Therefore, this portion of the side loads can be omitted but not the effect of the unsymmetrical pressure distribution in the computation of the side loads.

The third term concerns the wall pressure in the completely separated portion of the nozzle. In this section, p_a and p_w nearly agreed. For this reason, the side load of this nozzle /8 section, in case the separation does not occur in the throat area, is small and can be omitted+.

For the computation of the side load, therefore, it is only necessary to know the pressure distribution in the unsymmetrically separated area. Thus (1) can be simplified and the following can be written for the side load:

$$\vec{F}_{sl} = \int_{l_{fs_1}}^{l_{fs_2}} \int_0^{2\pi} (p_a - p_w) \cos\theta \, d\vec{A} \qquad (3)$$

The wall pressure in the full flowing portion of the unsymmetrical separation area (Figure 4, lower photo portion between l_{fs_1} and l_{fs_2}) varies slightly in the direction of the axis. Therefore, the variable wall pressure can be replaced by an average constant value. The pressure increase in the separation zone occurs so rapidly that a pressure jump from the wall pressure p_i to the external pressure p_a can be assumed. If the projection of the unsymmetrical full flowing portion of the nozzle flow perpendicular to the axis in the direction of the side load is designated with A_{sl}, then

$$F_{sl} \approx (p_a - p_i) A_{sl} \qquad (4)$$

+If the separation occurs in the throat area, then the side loads are small, but the proportion of the loads of the separated nozzle part are higher.

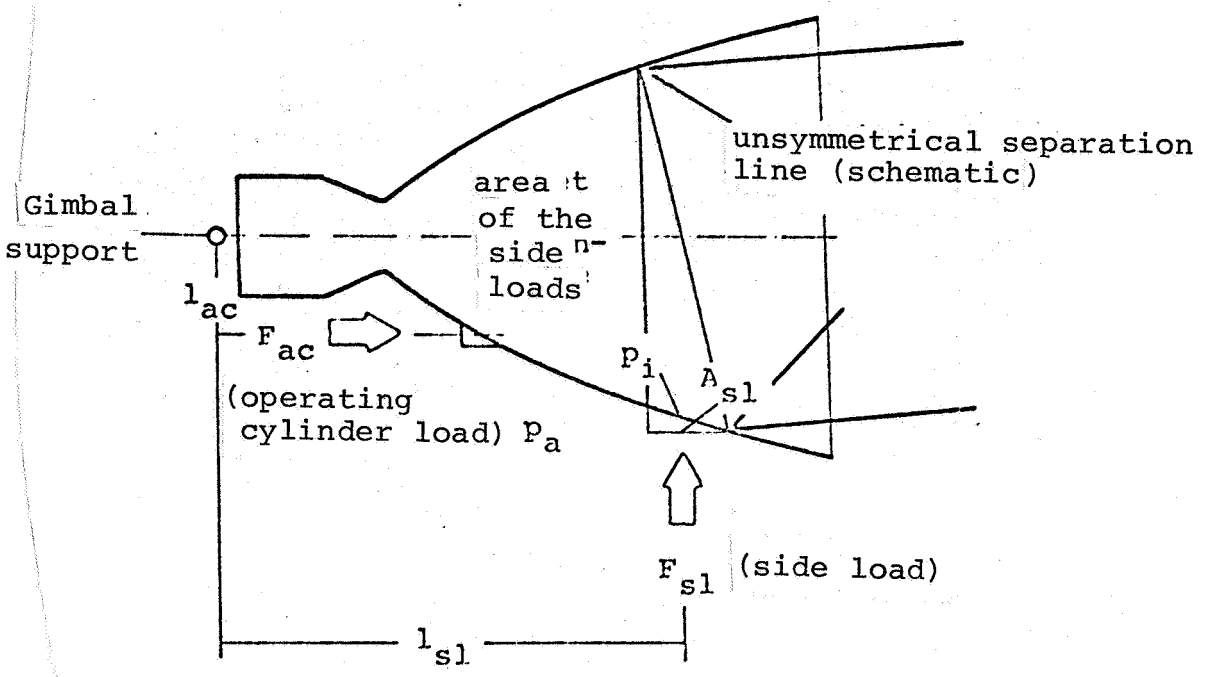

Figure 5. Simplified computation of the side load and operating cylinder load

can be given for (3) the simplified side load equation. In this case, p_i is the average nozzle wall pressure at which separation occurs (see Figure 3).

With the distance l_{ls} of the side load assault point from the gimbal joint and the distance of the operating cylinder l_{ac} for the operating cylinder load (see Figure 5), one gets:

$$- F_{ac} = F_{sl} \frac{l_{sl}}{l_{ac}} \qquad (5)$$

Equation (5) contains no unsymmetrical axial thrust portion. The side force acts in the direction of the nozzle axis on the side of the nozzle through unsymmetrical flow separation on which the flow is separated farther downward. The fire jet of the engine turned by the unsymmetrical separation line does not agree in its direction with that which resulted from thrust and side load since the side load is generated by the external pressure.

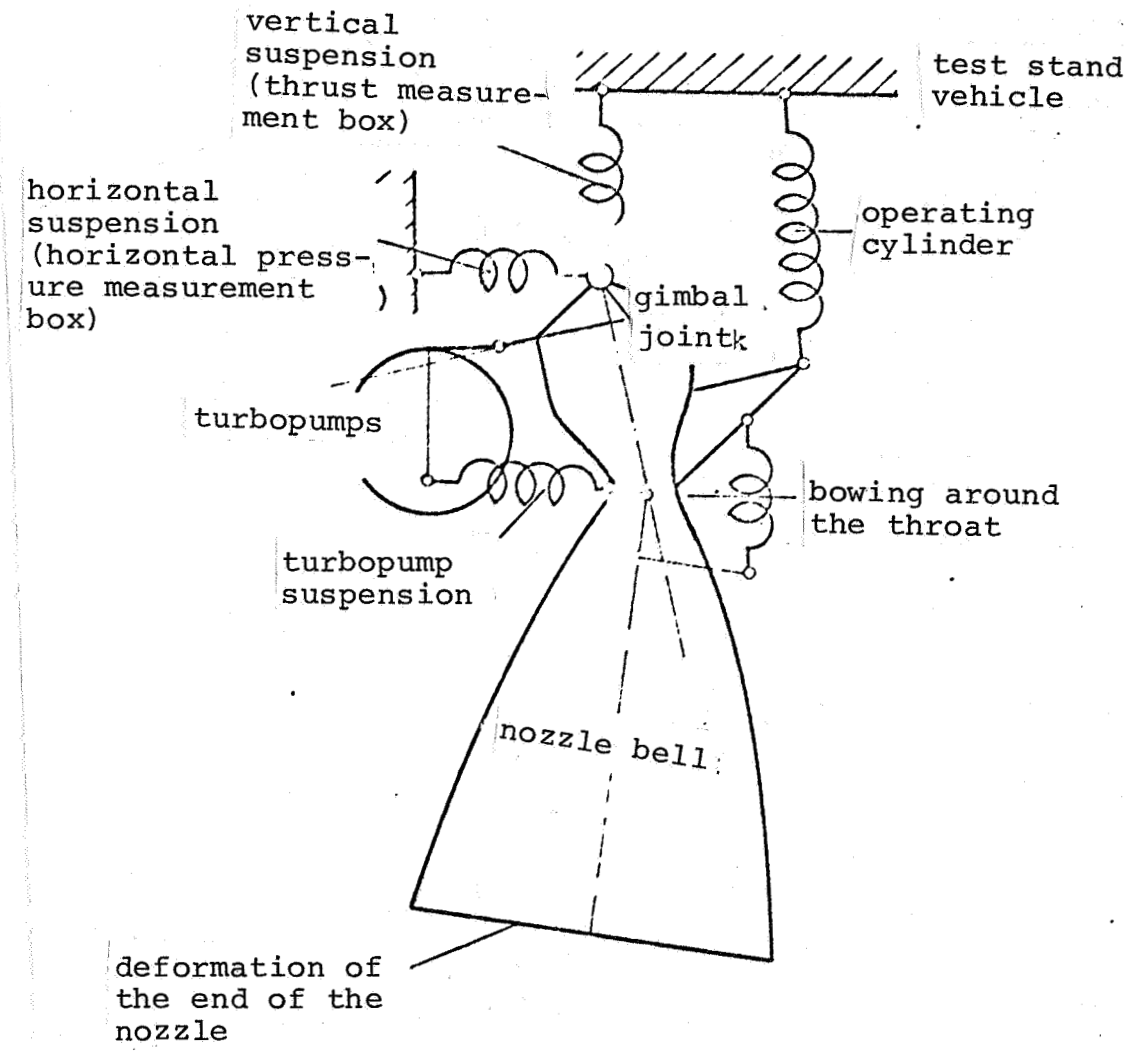

Figure 6. Deformation of the suspension and engine due to thrust and side load

The absolute value of the side load depends on the difference between the external pressure and the nozzle wall pressure and the size of the unsymmetrically separated area. The location of the load effect point is determined by the separation ratio of /10
the engine and the wall pressure distribution in the nozzle.

If one studies diagrams in which the elapsed time of the side load is shown (see Figure 1), then one recognizes that the side load is composed of two parts, a quasi-stationary and an oscillating part. This dynamic character of the side loads leads to considerable problems in the measurement.

2.2 Side load and machine dynamics

The rocket engine is normally suspended in the test stand or in the vehicle on a gimbal joint and on two operating cylinders for engine swiveling or on two side supports (outriggers). Since /11
the engine and the mountings are deformed under the thrust and side load stress, oscillations occur which can only be slightly dampened. Figure 6 depicts the deformations of the suspension and rocket engine schematically. The engine produces pendulum swings around the gimbal joint which are themselves slightly displaced as a result of the stress. The frequency of the oscillation is determined by the rigidity of the suspension of the operating cylinders. With the light construction design that is presently used for the engine with thin-walled individual tubes, the combustion chamber head can be considered as a rigid body up to the nozzle throat and the nozzle bell causes oscillations around the throat. Since the side load acts unsymmetrically on the nozzle wall, the end cross-section is deformed.

Depending on the rigidity of the end cross-section, there is an elliptical deformation or the loads lead to wave movements at the end of the nozzle [14,20]. Additional items such as turbopumps could also swing around their suspension on the engine.

The engine suspension system is a system capable of swinging with several degrees of freedom and appropriate swing frequencies. As a result of the oscillations from thrust and side load, the swings of the system are generated and due to the small natural damping (metal damping) there are strong increases in the reactions on supports in the resonance ranges.

Of these oscillations, the pendulum swing plays the greatest role. Figure 7 shows the amplitude spectra of the operating cylinder load of a J-2S engine. The frequency of the engine operating cylinder amounts to about 7 Hz. The amplitude spectra shows a strong increase of the load in this frequency range. At higher frequencies the load decreases sharply. In the operating cylinder load shown in Figure 1, one can virtually recognize only the frequency of this pendulum swing while the portion with higher frequencies is very small. At higher frequencies the amplitude spectrum varies considerably from the amplitude spectrum of a swing with one degree of freedom. Two other resonance peaks are shown. The increases at 22 Hz and 35 Hz (possible elliptical deformation of the end cross-section), however, can only be explained in more detail if the actual swinging action of the engine is known more specifically.

/12

2.2.1 Side load measurement

The measurement of the pure side load requires a considerably greater expenditure than for pure thrust measurement due to the dynamic characters of the load and the increase in the pressure on the suspension due to the engine movement, since with the latter only periodic values have to be determined which are nearly constant. Various methods can be used for the side load measurement.

2.2.1.1 Determination of the side load through integration of the wall pressure distribution

A method for determining the side loads is the measurement of the wall pressure at various points of the nozzle. For this

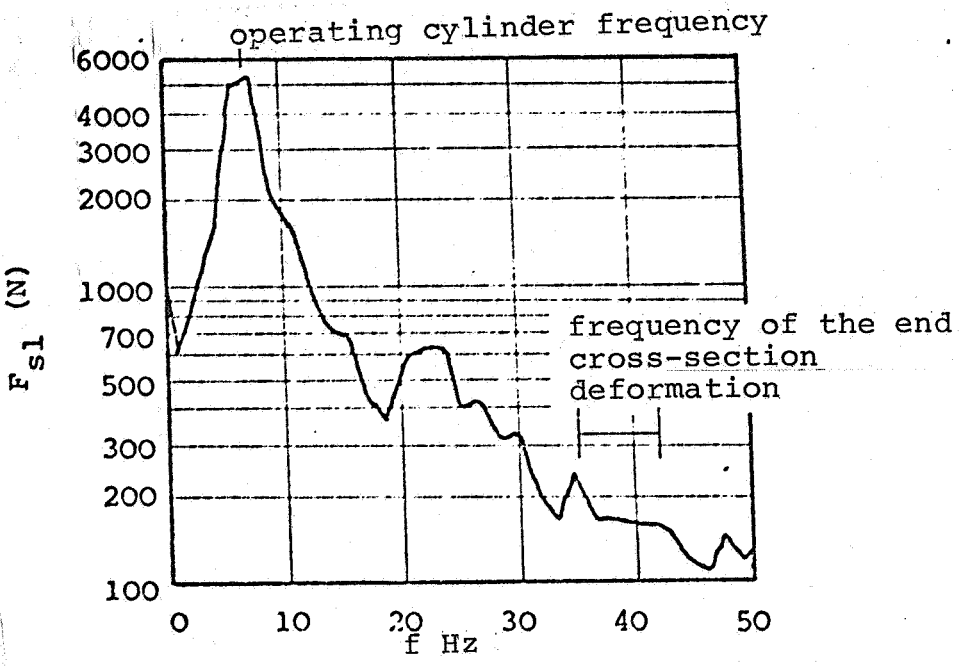

Figure 7. Amplitude spectrum of the operating cylinder load of a J-2S engine (p_c = 65 bar, p_e = 0.95 bar, bandwidth for the amplitude determination 1.6 Hz) [5,6]

two measurement devices that can be moved 180° are used. Figure 8 shows this procedure schematically.

If the pressure difference $p_{w_1}-p_{w_2}$ is determined at many stations along the axis of the nozzle and possibly also circumferentially, then the side load can be determined through numerical integration with equations (1). If one only has two series of measurement positions, then a sine distribution of the pressure can be assumed in the circumferential direction and the following is obtained:

$$\Delta F_{sl} = 0.5\ \Delta l\ r\ \pi\ (p_{w_1}-p_{w_2}) \qquad (6)$$

This method which is used in [19] is essentially dependent on the precision of the measurement recorder and the exact placement

/13

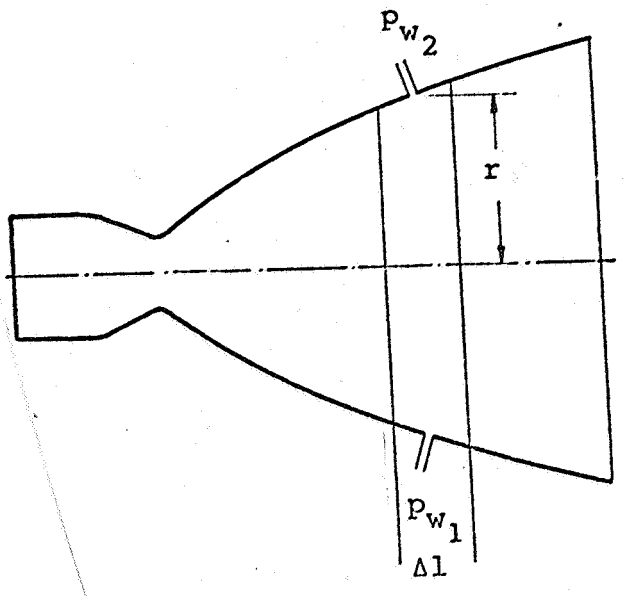

Figure 8. Determination of the side loads through measurement of the nozzle wall pressures.

/14

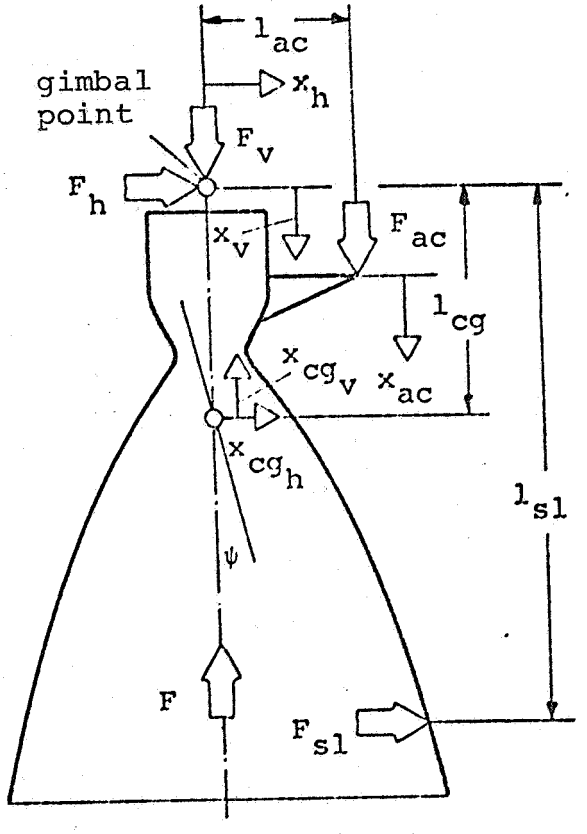

Figure 9. Determination of the side loads through simultaneous measurement of the reaction forces on the supports and accelerations.

of the measurement borings for its value. The errors arising in the computation of the side load could, therefore, be very large. Having too few measurement positions in the unsymmetrical separation area leads to unsatisfactory results.

2.2.1.2 High frequency reaction on support and acceleration measurement /14

A method for the immediate obtaining of side load values is based on the simultaneous measurement of loads and accelerations. Figure 9 schematically shows an engine where the vertical and horizontal reaction on the support loads F_v and F_h at the gimbal joint and the operating cylinder load F_{ac} as well as the accelerations at these points are being measured. This method enables the determination of the side loads without further detailed information on the oscillations of the engine.

If just one level is considered for simplification, then the movement equation is /15

$$m_{en}\,\ddot{x}_{cg_v} = -F_v - F_{ac} + F \qquad (7)$$

$$m_{en}\,\ddot{x}_{cg_h} = F_{sl} + F_h \qquad (8)$$

$$\Theta_{en}\,\ddot{\psi} = F_{sl}(l_{sl} - l_{cg}) - F_h\,l_{cg} - F_{ac}\,l_{ac} \qquad (9)$$

whereby m_{en} and Θ_{en} indicate the engine mass and the moment of inertia at the center of mass (cg). Thus, for the loads and the distance of the side load from the gimbal point one gets:

$$F = F_v + F_{ac} - m_{en}\,\ddot{x}_v \qquad (10)$$

$$F_{sl} = -F_h + m_{en}\left(\ddot{x}_h - \ddot{x}_{ac}\,\frac{l_{ac}}{l_{cg}}\right) \qquad (11)$$

$$l_{sl} = l_{cg} + \frac{-\Theta_{en}\,\ddot{x}_{ac}/l_{ac} - F_h\,l_{cg} + F_{ac}\,l_{ac}}{-F_h + m_{en}(\ddot{x}_h - \ddot{x}_{ac}\,l_{ac}/l_{cg})} \qquad (12)$$

The time span of the loads and the accelerations must also be measured exactly if it is desired to obtain the loads from (10) to (12). This, especially with the acceleration, does not present insurmountable difficulties [5,6,19]. Erroneous or non-available acceleration values lead to side loads in which the dynamic increases due to engine movement will be included in addition to the actual side loads. Therefore, side load values which are obtained in this manner must always be studied to determine whether all acceleration forces have actually been eliminated.

This method is used in [5,6]. The results are for the most part erroneous. The cause is probably not the rough simplification of the engine model assumed in [5] but the result of an erroneous (or missed) acceleration measurement or false numerical handling of the measurement values since the side loads that do not consider the acceleration differ only insignificantly from those with the influence of the acceleration.

2.2.1.3 Evaluation of amplitude spectra /16

The average side load values of a sufficiently long testing session with constant conditions can be obtained from the evaluation of the amplitude spectra of the reaction on the supports if the dynamic action of the engine and test stand are known. Then an amplitude spectrum is determined from the time lapse of the support stress as is shown in Figure 7. The vibration action of the engine, the amplitude of the reaction on the supports with the given dynamic load, can be obtained with two different methods. One is the establishing of a mathematical model of engine and test stand as is schematically shown in Figure 6 in which all elasticity constants and dampings are known [14]. In any case, it is rather difficult to reach the high accuracy in the resonance ranges which can clarify the questions such as self-generation of the oscillations. The other method is a calibration of the test installation with a jolt ramming machine [5]. For

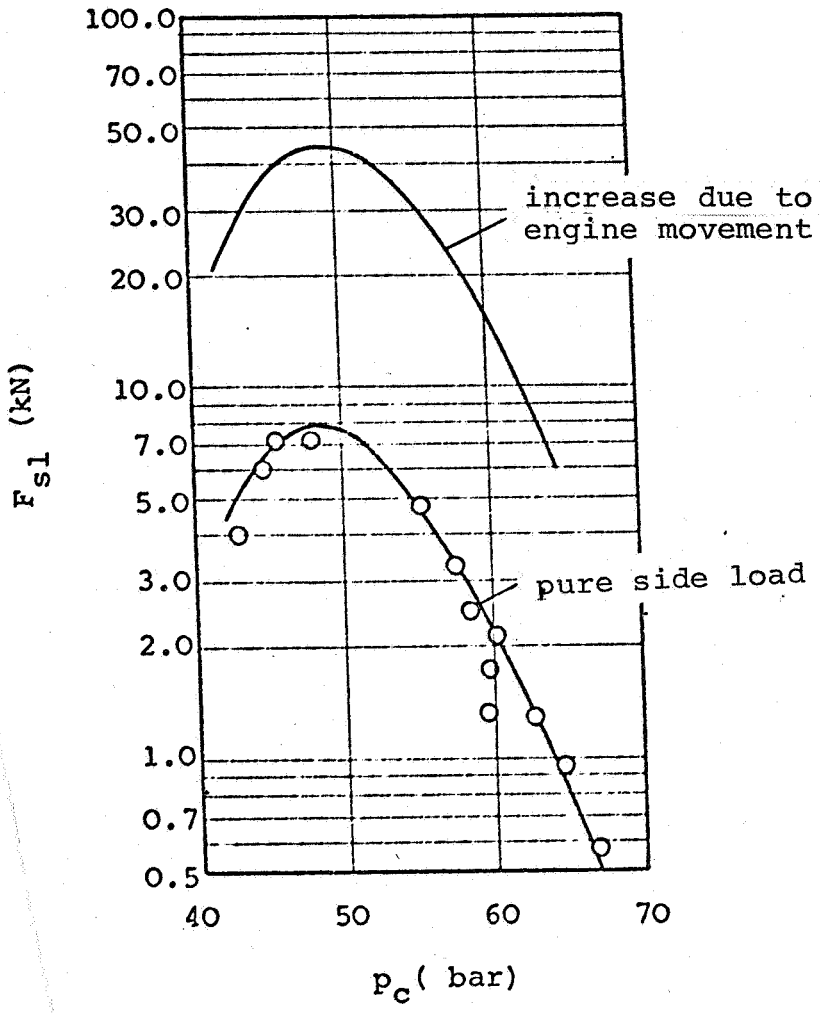

Figure 10. Side loads with the J-2S engine with and without consideration of the influence of engine movement.

this a nozzle is vibrated at various positions with a sine-shaped force of given amplitude and frequency and at the same time the reaction on the supports is measured. Thus, one knows the transmission function of the system and from the measured amplitude spectrum of the test session can compute the actual side load.

These methods are used in [5] since an evaluation was not successful using the method in paragraph 2.2.1.2.

2.2.1.4 Comparison of side load data with and without consideration of the influence of the engine teststand dynamics

The danger of an erroneous measurement of the side load because the engine-teststand-dynamics was not considered was already known in the first side load analyses of the J-2 engine (E. K. Bramnlett (1965 [14]). The increase factor of the reaction on the supports of 2 (fault generation) obtained based on model tests with and without oil damping [14] is much too small /17
according to new measurements. Figure 10 shows a comparison of the side load with the J-2S engine which must be determined through engine movement with and without an increase. The increase factor amounts to about 6 and is clarified by the small damping (metal damping) of the system.

With the help of experimental side load data, it must, therefore, be determined whether the dynamic loads have been subtracted. Values of the same swing system that have not been reduced can only be used to examine the influence of various parameters but not for quantitative statements.

/18

2.2.2 Self-generation of the side load through machine vibrations

The possibility exists that the vibrations of the engine and teststand can lead to self-generated side loads. This question is not only important for the starting procedure, but also during the first phase of flight at lower altitude. The tilting of the engine due to the operating cylinder could cause side loads due to the vibrations that occur which endanger a normal flight.

The acceleration of the nozzle perpendicular to the axis leads to wall pressure alterations which move the separation point. This alteration, however, is very small and can be disregarded for the side load.

Nozzle bendings around the throat could have a great effect. This increases the wall pressure on one side of the nozzle so that the separation point moves downward. The surfaces of the unsymmetrical separation that are enlarged as a result of this increases the side load and moves the nozzle further in the direction of asymmetry. The size of this self-generated side load would depend on the rigidity of the nozzle and the wall pressure distribution.

J-2S measurements show that with this engine configuration possible self-generations are smaller than the measurement accuracy. There are no measurements available on other nozzle types.

2.3 Experimental side load results

Side load information is available from various sizes of rocket engines with bell nozzles and some model engines which are driven with hot and cold gas. In contrast to the pure flow separation measurements for which there is a considerable amount of reliable data available, the number of side load values is rather small. Of these many are erroneous due to unsatisfactory measurement and only usable for qualitative statements.

2.3.1 Sources of experimental side load and unsymmetrical separation data /19

The various sources of side load information for large chemical engines and the applicable engine parameters are given in Table 1. It shows that side loads were measured with nearly all large engines.

The sources of side load data and measurements of unsymmetrical separation methods in model engines with cold and hot gases are listed in Table 2. The diameter of the throat and the opening ratio of the nozzle are given as measurements for the size of the

Source	Propellant	F (kN)	p_c (bar)	ε
Atlas sustainer S-4 (Rocketdyne) [2,7]	O_2/benzine	270	40	25
Saturn F-1 (Rocketdyne) [13]	O_2/benzine	6700	65	10
Titan III B (Aerojet) [2]	N_2O_4/UDMH	1000		12
Saturn J-2D (Rocketdyne) [14]	O_2/H_2	1000	45	27.5
Saturn J-2S (Rocketdyne) [6,14]	O_2/H_2	1200	82	40
250 k Phase B High pressure engine (Pratt & Whitney Aircraft)[12]	O_2/H_2	1130	190	53.2

TABLE 1. Listing of the sources of side load data of large chemical engines and the applicable engine values.

F = thrust

p_c = combustion chamber pressure

ε = opening ratio of the nozzle

engine used in the experiments. The tests were carried out at atmospheric environmental pressure [10,11,19] or with a very reduced external pressure [14].

2.3.2 Influence of various parameters on the side load action of an engine

Side loads originate in the operating phase of the engine in which the flow in the nozzle is separated. The intensity of the side load for a given rocket engine depends on the actual value of the pressure relationship of the combustion chamber pressure to the environmental pressure.

Figure 11 also gives the mean side load of a J-2S engine using the pressure ratio. The values are the effective side load

Source	Fuel	d_t (cm)	ε	shape of nozzle
Lawrence [10]	air	0.25 - 0.65	6-23	2-d, 3-d conical, bell-shaped
MacAbee Jr. (Pratt & Whitney Aircraft) [11]	N_2	1.57	10-100	bell-shaped
	O_2/H_2	1.51	35-80	bell-shaped
Rocketdyne [14]	N_2	2.3	27.5,40	bell-shaped
(J-2 model) [16]	O_2/H_2			bell-shaped

TABLE 2. Listing of sources of side load data and studies of unsymmetrical separation methods in model engines.

d_t throat diameter
2-d two-dimensional
3-d three-dimensional

without any increase due to the engine movement. The data at low pressure ratios are obtained during the launch phase [5]. Since the extraction of the dynamic loads in this range were only achieved with the increase factor 6, these values are very inexact. The measurement points at higher pressure ratios were obtained using the method described in paragraph 2.2.1.3.

At low pressure ratios, the flow separates directly behind the throat of the nozzle and the side loads that develop are small. An increase of the pressure ratio increases the side load and at a specific pressure ratio there is a first side load maximum. The value of this load depends on the nozzle contour; the figures for the pressure ratio are between 5 and 20 [10,14]. The cause for this side load maximum is still not completely clear. It can be assumed that the separated jet hit again downward on the nozzle wall since the nozzle contour is bent inward in the direction of the nozzle end. In the wider area of the pressure ratio the side load increases sharply.

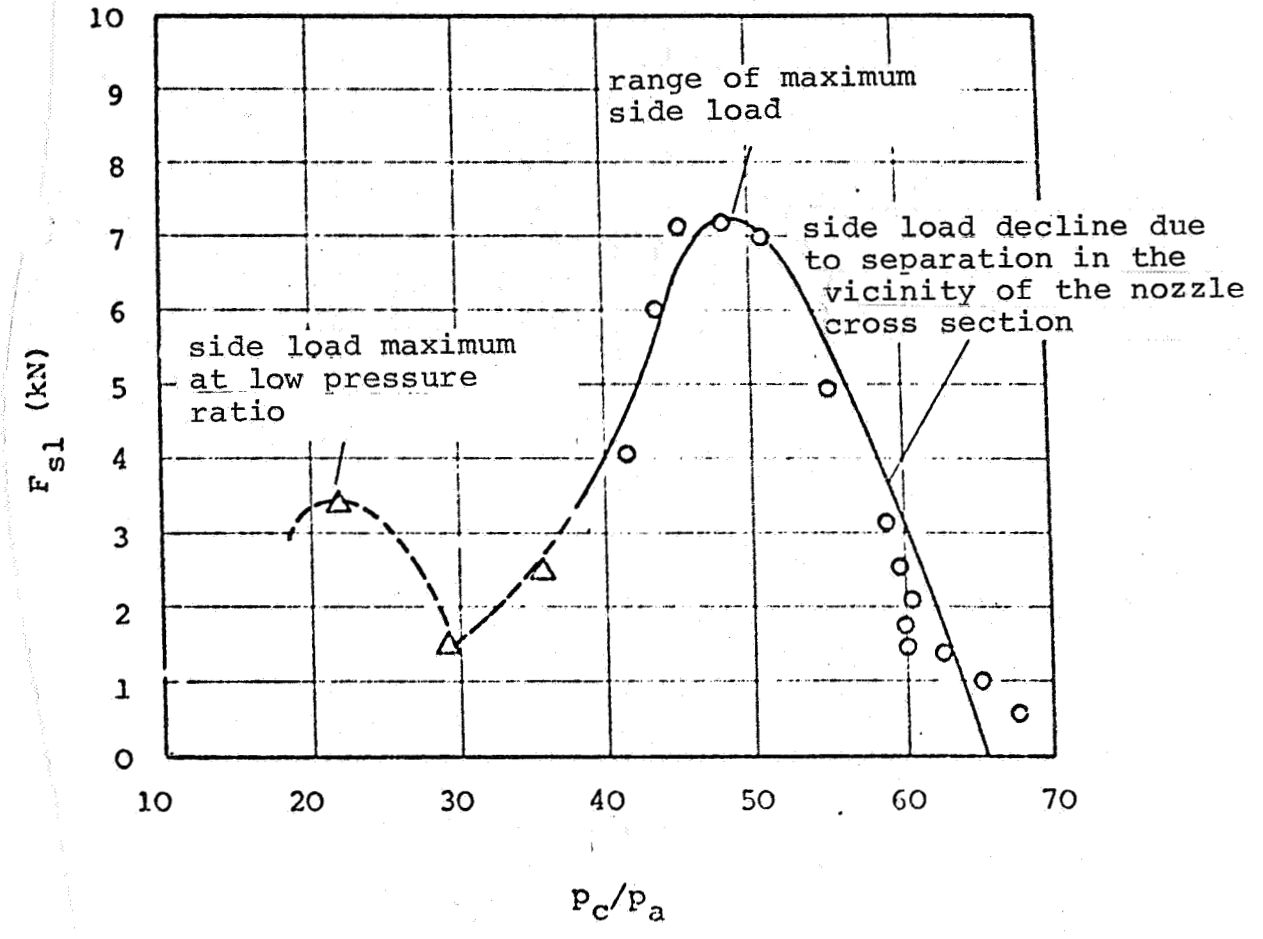

Figure 11. Side load of the J-2S engine as a function of the pressure ratio [5].

Measurement points during the retarding of the engine
Measurement points during the start phase

The actual side load maximum develops with a pressure ratio which is somewhat lower than that of the fully flowing nozzle. A further increase of the pressure ratio leads to a flow separation in the immediate area of the nozzle end cross-section. This reduces the side load since the unsymmetrically separated area

Engine	F_{ac} (kN)	$\frac{F_{sl}}{F}$	Remarks
Atlas sustainer	136	0.2	strong pressure vibrations during the start phase
J-2D	1050	0.24	engine retarding
	680	0.16	launch phase
J-2S	420	0.1	maximum value with engine retardation
	60	0.01	average side load without engine movement
F-1		0.01	
Titan III B	217		
250 k phase B high pressure engine		0.04	final combustion phase

TABLE 3. Side load and operating cylinder load including the increase due to engine movement of large rocket engines

can no longer develop fully. Finally, the nozzle flows at full force and the side loads become insignificant.

This action of the side load with altered pressure ratio occurs in a similar manner for all engines. Only the second load maximum is critical for the design of the rocket engine. This side load represents the greatest cross load of the engine which works on a moment lever which corresponds to the distance from the gimbal point to the nozzle end.

Table 3 lists the maximum side loads which were measured for the engines in Table 1. All data, with the exception of the J-2S values, are increased by the dynamics of the engine movement. Therefore, the values can only be used for a qualitative comparison. There are especially high side loads for the Atlas sustainer engine and for the J-2D engine.

The intensity of the maximum side loads is influenced by the nozzle contours. For this reason, Figure 12 shows the wall pressure distribution and the nozzle contour of various cold gas nozzles.

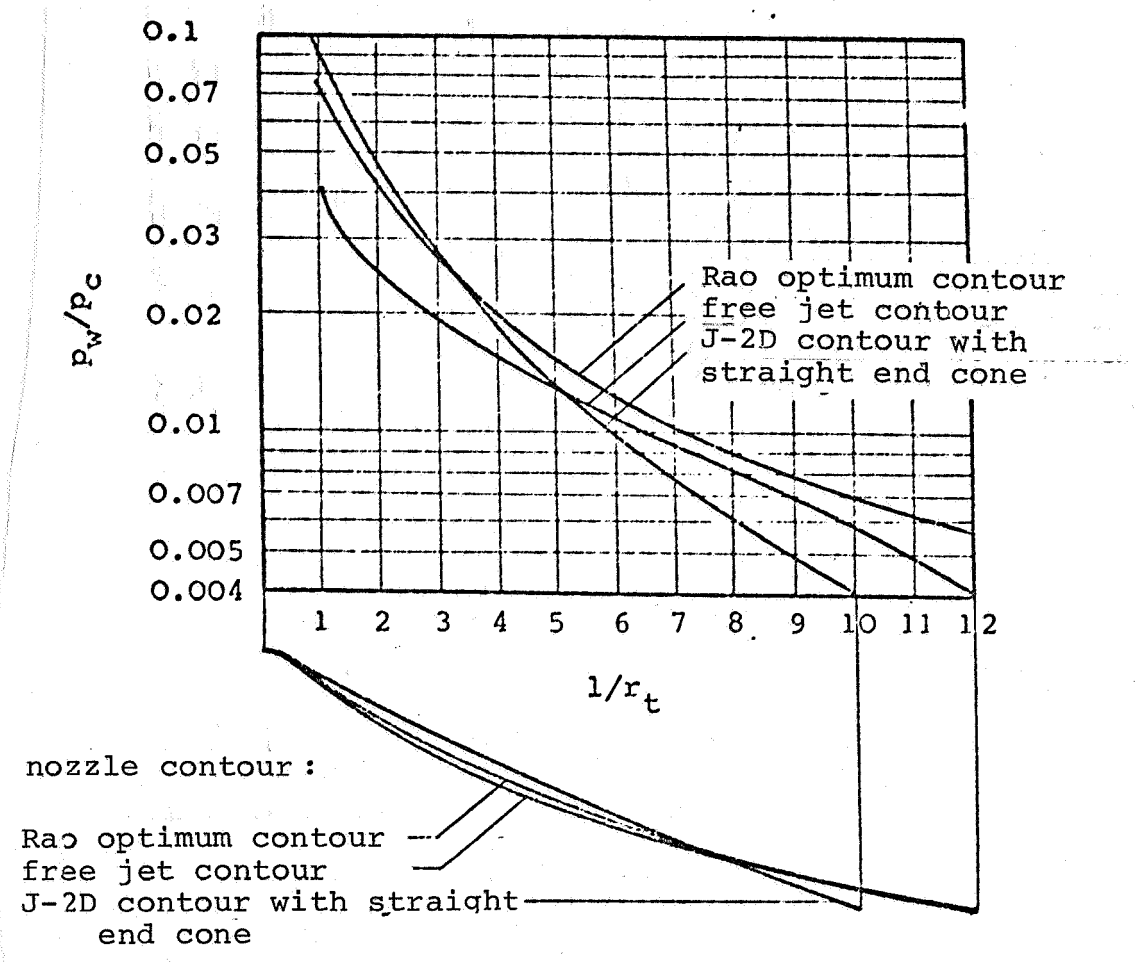

Figure 12. Wall pressure distribution with nozzle contour of various cold gas nozzles with an opening ratio of 27.5 [14].

jet contour	F_{ac}/F
Rao optimum contour	0.7
free jet contour	0.4
J-2D with straight end cone	0.15

TABLE 4. Standardized operating cylinder load (including dynamic increase) of various cold gas nozzles [14].

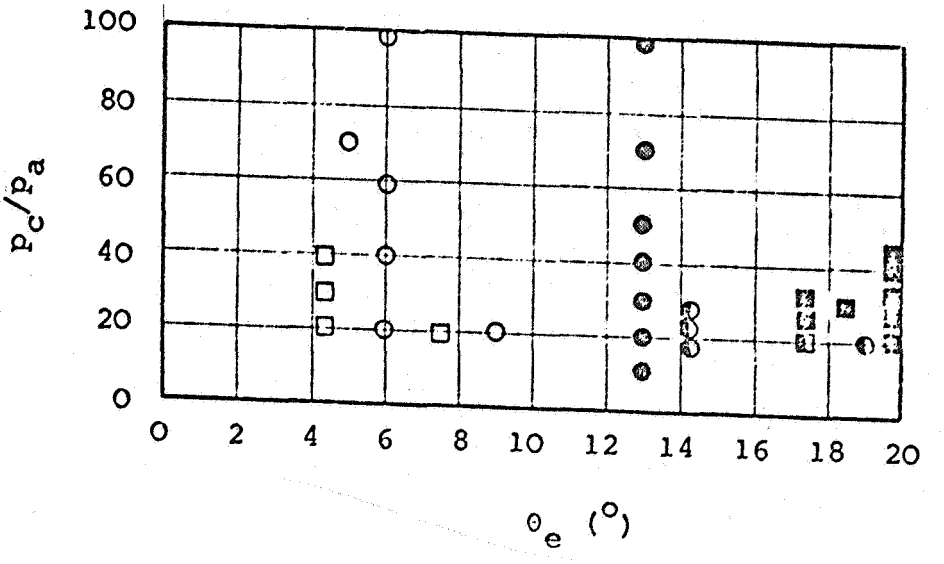

Figure 13. Influence of the nozzle divergence angle on the stability of the exhaust jet (open symbol: strong oscillation, half closed symbol: small oscillation, dark symbol: stabile jet) [11,19]
cold gas nozzle hot gas engine (H_2/O_2)

The applicable operating cylinder load (including the dynamic increase), standardized with the engine thrust, is given in Table 44.

The values in Tables 3 and 4 clearly show the influence of the nozzle contour on the side load. With increasing pressure gradients $d(p_w/p_c)/d(l/r_t)$ in the nozzle, the side load decreases; low pressure gradients or retrograde pressure distribution (Atlas sustainer, J-2D nozzle) are inclined toward very high side loads.

This action can also be qualitatively observed on nozzles that have different angles of divergence. Figure 12 contains data on the oscillation of the exhaust jet of hot and cold gas nozzles with different angles of divergence. The dark symbols indicate a stable exhaust jet. A higher divergence angle which normally leads to a greater pressure gradient in the nozzle (with approximately the same pressure drop the length of the nozzle becomes smaller), causes smaller oscillations of the exhaust jet than a lower angle of divergence.

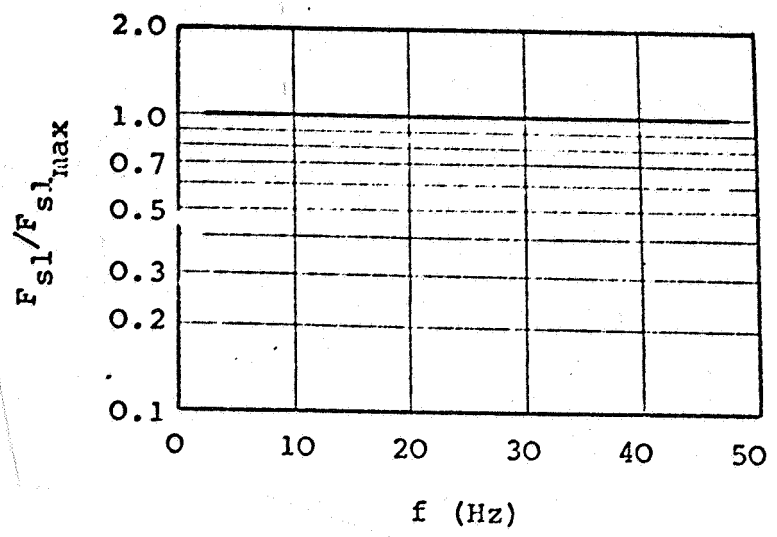

Figure 14. The amplitude spectrum of the side load of the J-2S engine 5

Frequency measurements of the side loads indicate that the amplitude spectrum is rather flat in the range between a few Hz and 50 Hz [5]. Figure 14 schematically shows this amplitude spectrum of the J-2S engine. The amplitudes above 50 Hz probably increase very rapidly+.

Cold gas and hot gas data did not agree quantitatively. Figure 15 shows the pattern of the operating cylinder load (including the dynamics increase) of a J-2S engine and the converted values of a cold gas model nozzle. The model nozzle has the largest side loads with a very low pressure ratio. These peaks can be caused by separation and reapplication. The second side load maximum of the cold gas test occurs with a pressure ratio which corresponds to that of the hot gas tests. In any case, the maximum values differ considerably from each other.

+The pattern of the amplitude spectrum shown in [15] deviates considerably from that of Figure 14. The amplitude peak at about 20 Hz is the result of an erroneous evaluation of the experiments.

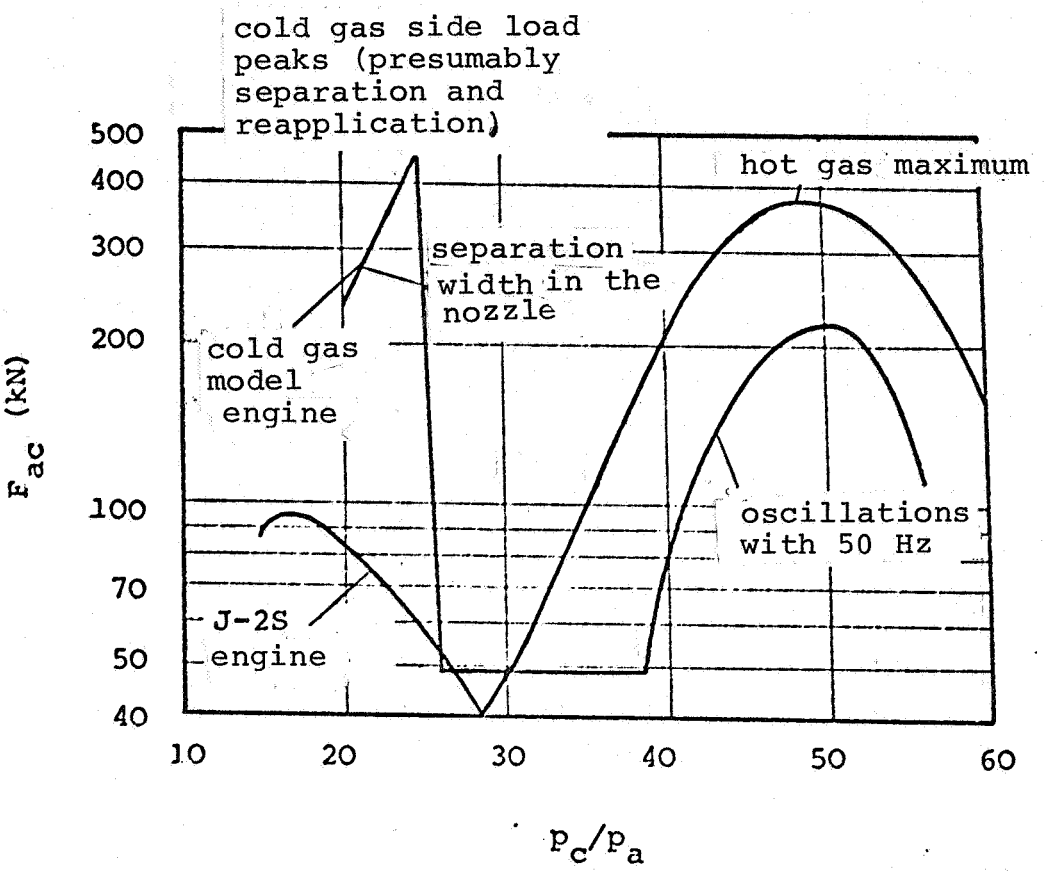

Figure 15. Comparison of the operating cylinder load with a J-2S engine between hot gas and cold gas model data [5,14].

- boundary layer development
- flow conditions toward the nozzle throat

The following parameters can cause the differences between hot gas tests in large engines and cold gas model experiments:

- isentrope exponent (wall pressure distribution)
- structural suspension of the engine
- separation action

Therefore, one cannot quantitatively come to the expected values with large rocket engines without further information.

2.3.3 Characterization of side loads

The available experimental data on side loads can be summarized into the following characterizations:

- Side loads are non-stationary loads on the nozzle which is caused by unsymmetrical separation of the flow.
- The size of the side loads depends on the surface of the unsymmetrically separated area and the difference between external and nozzle wall pressure.
- Tests with large engines and cold gas model nozzles do not agree quantitatively.
- The measures side loads are nearly always increased by the dynamics of the engine movement. The forces resulting from this can be wrong by more than 500%. At present, the only pure side load data available is for the J-2S engine.
- With increasing pressure, gradients along the nozzle axis, the side loads become smaller.
- The side load maximum occurs with a pressure ratio which is somewhat below that of the full flowing nozzle.
- The amplitude spectrum of the side load has a rather flat pattern.

3. COMPUTATION OF THE SIDE LOAD /28

The simplified side load equation (4) is

$$F_{sl} \approx (p_a - p_i) A_{sl}$$

To compute the side load, the pressure difference between the external and the nozzle wall pressure of the separation area and the size of the unsymmetrically separated area must be determined. While the pressure difference can be expressed with a good approximation by the separation pressure ratio p_i/p_a with a symmetrical separation, for the determination of the unsymmetrical separation area a mechanism must be found which explains the unsymmetrical separation.

3.1 Overview of the most important models for side load development

Based on the phenomenon described in paragraph 2 and measurements of the side load, various mechanisms have been recommended to clarify the unsymmetrical separation. The most important models, which are listed in Appendix A, have the following characteristics:

- Laminar and turbulent separation (Lawrence [10]): Unsymmetrical laminar and turbulent separation can only occur in small model engines. The side loads that develop are stationary.

- Various separation angles of the flow and unsymmetrical pressure distribution down from the separation point which leads to an unsymmetrical separation line (Lawrence [10], Pratt & Whitney Aircraft [12]): The influence of lower separation angles on the separation pressure is very small [18]. The computed side load values do not reflect the difference of the various nozzle contours. /29

- Separation and reapplication (Aerojet Liquid Rocket Company) [1,2]): The process of the separation and reapplication has only been observed with small engines until now [18]. With larger engines this phenomenon was not observed.

The pressure ratio at which the maximum side loads occur is well reflected. The computed loads are considerably above the measured effective values. The influence of various contours on the size of the side load is not reflected by this model. The side loads are rather independent of the contour.

- Empirical correlation for an inclined separation line (Rocketdyne [13-15]):

This model leads to a conversion method from the side load of an engine to another one. This method, however, cannot clarify the high side loads of the J-2D engine.

3.2 Side load due to fluctuation of the separation point and due to unequal nozzle flow

3.2.1 Experimental bases of the fluctuation and flow unsymmetrical side load model

Side loads can be divided into two portions, a quasi-stationary and an oscillatory portion. Both components are shown in Figure 1. For this the oscillating loads are especially increased by machine dynamics. These side loads could be explained by a fluctuation of the separation point and an unequal easing of the gas in the nozzle phenomenistically or quantitatively. The causes for these phenomena are:

- Fluctuation of the separation point
  - statistical variations of the separation point
  - turbulent variations of the boundary layer
  - oscillations of the nozzle wall pressure through
    - -combustion chamber pressure oscillation
    - -incoming flow of the environmental air
  - chemical reaction in the boundary layer
- Unequal pressure drop in the nozzle
  - design error in the engine
  - unequal flow conditions to the throat of the nozzle.

3.2.1.1 Fluctuation of the separation point

The fluctuation of the separation point is responsible for the oscillatory side loads.

Low frequency wall pressure measurements on a known position of the nozzle in an engine with flow separation show that with a

/30

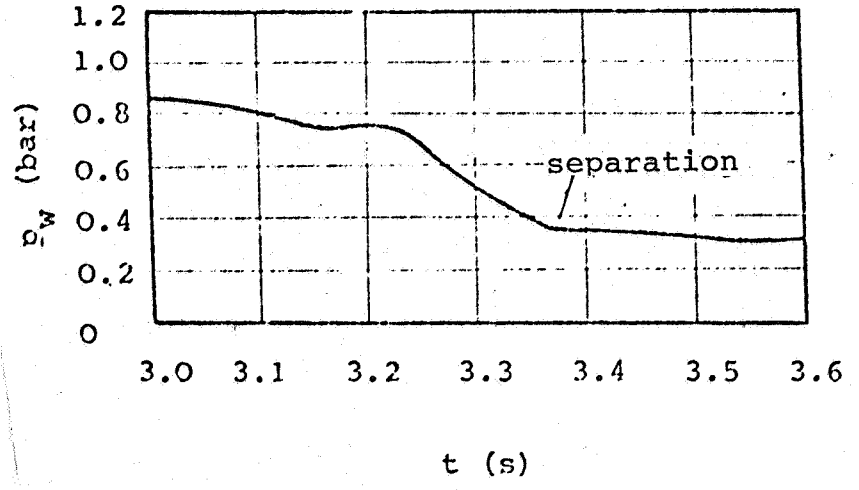

Figure 16. Low frequency wall pressure measurement in the J-2D nozzle during the start process (high frequency pressure values are numerically even) (Test S-IVB 125)

change in the combustion chamber pressure, the separation point moves according to the pressure. Figure 16 shows this action. The wall pressures do not show any oscillations and each momentary combustion chamber pressure can be ascribed to a specific nozzle wall pressure. This method is used to determine the separation action of engines [18].

If high frequency wall pressure measurements are carried out, then this picture alters sharply. Instead of a smooth pressure pattern, there are the characteristic oscillations of the wall pressure. Figure 17 shows the time pressure pattern during the start process of a J-2D engine. The measurement position is the same as in Figure 16. The wall pressure in the cases with separated flow oscillates very sharply. The upper pressure value /31 almost reaches the environmental pressure, and the average pressures are between 0.9 and 0.7 p_a. These pressure oscillations have no dominating frequency. Wall pressure measurements at various places in a circumferential direction with the same pressure release ratio show that the oscillations are almost synchronized. An exact statement on the amplitude distribution is not possible

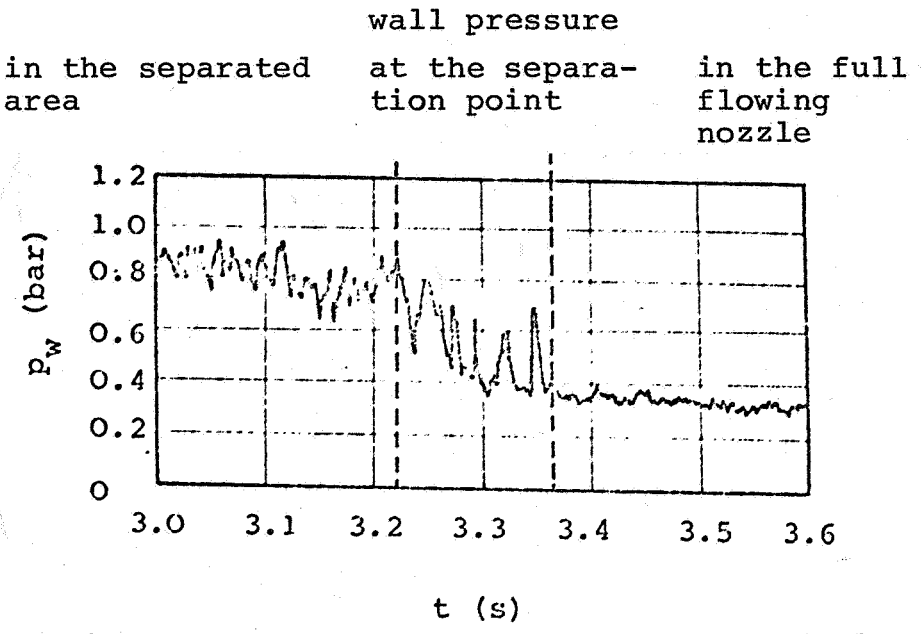

Figure 17. High frequency wall pressure measurement in the J-2D nozzle during the start process (Test S-IVB 125) (Oscillation of the wall pressure in the separated area, at the separation point, and in the full flowing nozzle).

due to the errors of the measuring device and the small pressure differences.

The pumping up of the measurement point with flow separation occurs almost by leaps and bounds, and during a specific time span separation and thrust of the flow occur several times in sequence. The pressure measurements could be interpreted so that the separation point moves to and fro several times across the measurement point. The separation at a specific combustion chamber pressure, therefore, does not occur, as assumed for simplification for the determination of the separation pressure according to Figure 16, at a precisely defined point of the nozzle, but within a specific range Δl_{fl}.

/32

The separation point oscillates with alternating frequency in this range. Wall pressure measurements in a circumferential direction show that the oscillation of the separation point is not synchronized. Figure 18 shows the timed wall pressure patterns

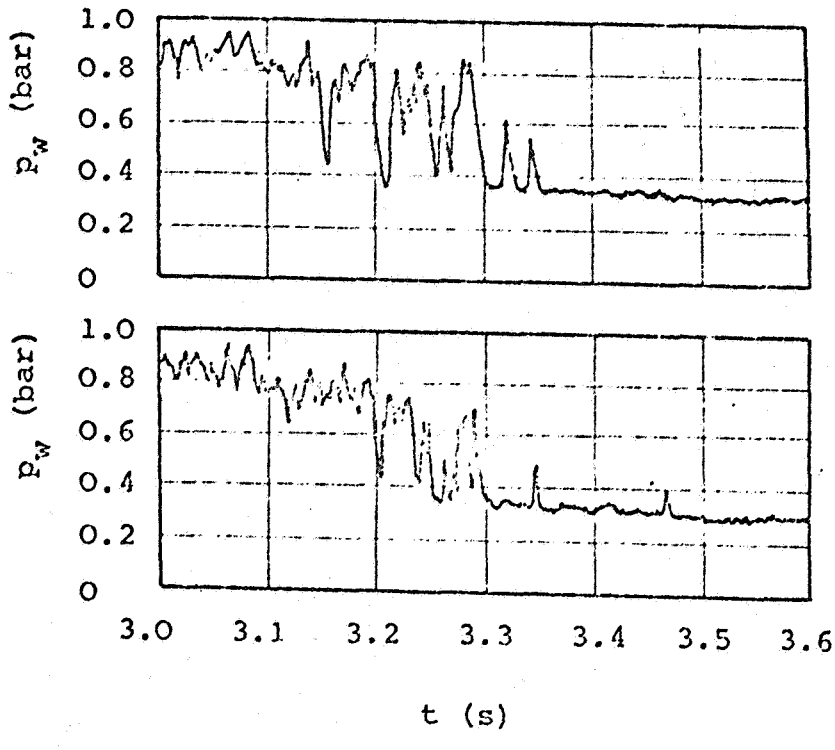

Figure 18. Time pattern of the wall pressure at two measurement points at 135° ($l/_{r_t}$ = 7.78) (Test S-IVB 125)

of two measurement points moved by 135°. Frequency as well as amplitude differ.

The wall pressure of the full flowing nozzles also oscillates.

Wall pressure measurements which were carried out by A. L. Kistler [8] in the separation area of a supersonic flow on one stage, show the same action[+].

[+]These oscillations are not observed with oil film measurements and schlieren photography. This is because the oil film techniques only yield average separation and with schlieren photography the differences are equalized to an average photo due to the width of the field of flow.

The oscillations increase with an even flow with increasing size of the separated area. The measurements by D. M. Kuehn [9] with separation on a wedge indicate that with a small separation area, the oscillations are negligible, but with a large area high variations are caused. /33

Side load measurements in an engine with full flowing nozzle yield small oscillatory loads. They are caused by unsymmetrical wall pressure oscillations. This unsymmetrical pressure distribution also causes an unsymmetrical, oscillating separation line with flow separation.

3.2.1.2 Unsymmetrical nozzle flow

In addition to the oscillations of the separation point, there are also static deviations in the separation line from the symmetry. The wall pressure pattern shown in Figure 18 indicates that at various points on the nozzle wall with the same axial position, the start of the flow separation occurs at various times. These differences are caused by unsymmetrical nozzle flow.

Every engine exhibits design errors. This applies especially to the light construction design with thin-walled pipes for the cooling. These errors effect the radius of curvature at the throat, the straightness of the nozzle axis and the rotation symmetry of the nozzle wall. Unsymmetrical pressure distributions arise as a result of this which disrupt the symmetric separation line. With a full flowing nozzle, these design errors are shown by a deviation of the thrust vector axis from the geometrical nozzle axis.

Tests by W. Buschulte and K. Schadow [4] have shown that with a very carefully constructed nozzle with full flowing flow cross thrust components occur. The causes of this action are unsymmetrical flow conditions before the nozzle throat. Liquid engines have

constant deviations from a uniform fuel injection. Therefore, unsymmetries in the total pressure and enthalpy distribution arise which lead to movements in the separation line via the unsymmetrical wall pressures.

/34

Cold gas model tests could be carried out much more carefully with fewer disturbances than hot gas tests with large engines. This will reduce the fluctuations of the separation point, and the unsymmetry of the flow and the side loads determined in the experiment are reduced.

3.2.2 Computation methods for the side load

For the computation of side load of a nozzle with normal pressure gradients along the wall, the fluctuation of the separation point and the unsymmetrical pressure release in the nozzle can be considered together. (For the special case of a nozzle with retrograde pressure gradients (J-2D engine, Atlas sustainer) a separation is appropriate for a qualitative understanding of the effects (see paragraph 3.2.3)).

The normal separation point with a specific combustion chamber pressure is indicated by the separation pressure ratio p_i/p_a of rocket engines and the nozzle wall pressure distribution [18]. The experimental data provide the separation point to where the flow in the nozzle flows fully and symmetrically. The unsymmetrical separation area is located above this point.

The flow separation criterium p_i/p_a is obtained from experimental and theoretical examinations. In Figure 19, the available averaged experimental data on chemical rocket engines is compiled. A simple empirical equation for the separation pressure is:

$$\frac{p_i}{p_a} = (1.88\,M_i - 1)^{-0.64} \qquad (13)$$

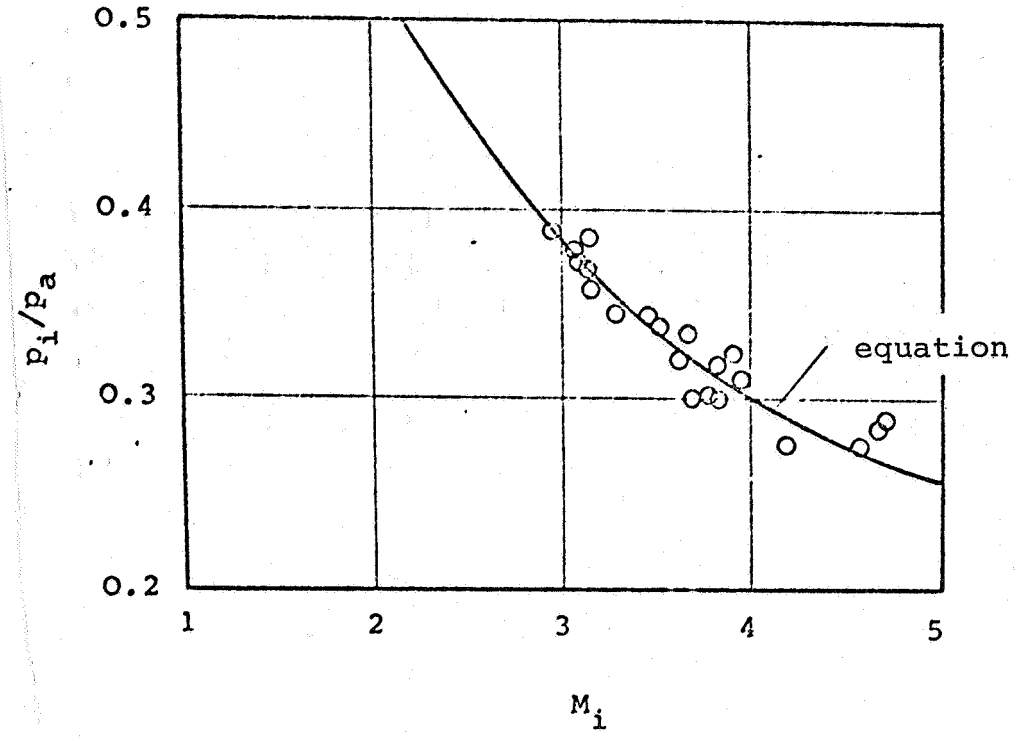

Figure 19. Averaged experimental flow data for chemical engines [18].

The Mach number M_i at the point i (starting point of the separation area) can be obtained from the combustion chamber pressure and the isentrope exponent by

$$M_i = \{\frac{2}{\gamma-1}\left[\left(\frac{p_c}{p_i}\right)^{\frac{\gamma-1}{\gamma}} - 1\right]\}^{0.5} \qquad (14)$$

From the wall pressure distribution p_w/p_c along the axis and the criterion (13), the position of the symmetrical separation line can be determined as is shown in Figure 20. The fluctuations from the separation criterion and the nozzle wall pressure as well as the pressure unsymmetry are also indicated.

For the computation of the length of the unsymmetrical area, it is only necessary to consider term 1 since higher effects in the scope of the achieveable exactness could be disregarded.

If a fluctuation coefficient K_{fl} is defined in which there are oscillation and unsymmetry, then there is a mathematical unsymmetry of the wall pressure Δp_w as

$$\Delta p_w = K_{fl} \frac{p_w}{p_c} p_c \qquad (15)$$

This mathematical pressure unsymmetry would be necessary in order to reach an unsymmetry with an ideal nozzle with stable (non-oscillating) separation point which corresponds to the entire fluctuation. A portion of this pressure actually occurs.

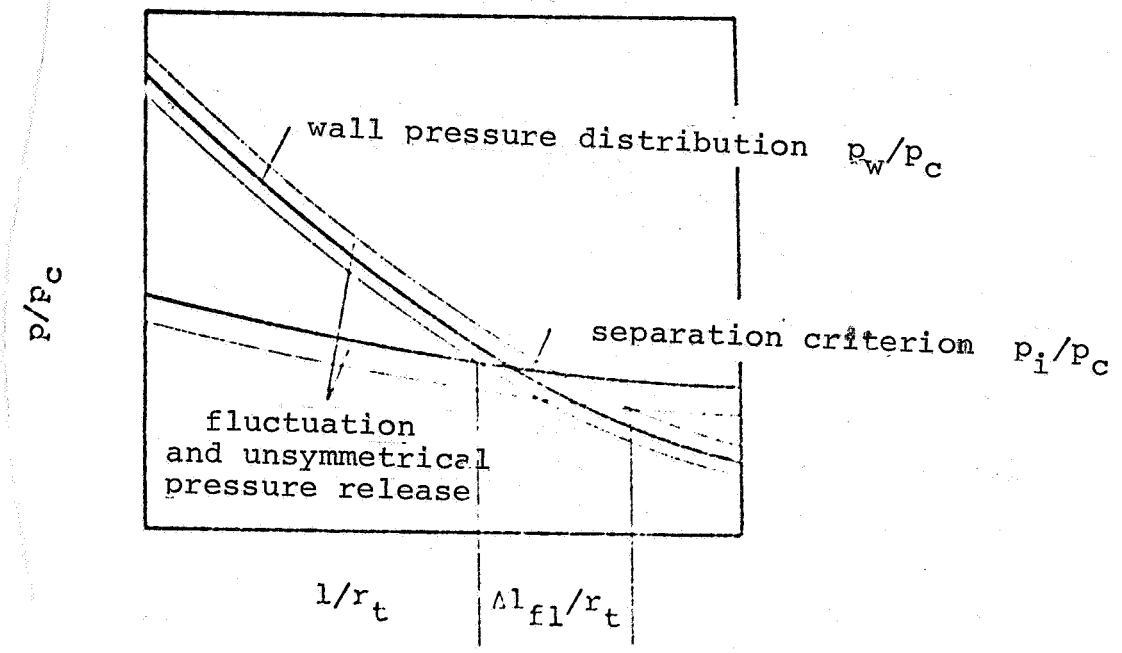

/36

Figure 20. Computation of the length of the unsymmetrically separated area.

The length of the unsymmetrically separated area if obtained from the angle of intersection of wall pressure and separation criterion.

$$\Delta l_{fl} = \Delta p_w \frac{r_t}{p_c} \frac{1}{\frac{d(p_w/p_c)}{d(1/r_t)} - \frac{p_a}{p_c} \frac{d(p_i/p_a)}{d(1/r_t)}} \qquad (16)$$

For the separation pressure, one can write

$$\frac{d(p_j/p_a)}{d(1/r_t)} = \frac{d(p_w/p_c)}{d(1/r_t)} \frac{d(p_i/p_a)}{d(p_w/p_c)} \tag{17}$$

$$= \frac{d(p_w/p_c)}{d(1/r_t)} \frac{d(p_i/p_a)}{dM_i} \frac{dM_i}{d(p_w/p_c)} \tag{18}$$

If (18) is evaluated with (13) and (14), it yields: /37

$$\frac{d(p_i/p_a)}{d(1/r_t)} = \frac{d(p_w/p_c)}{d(1/r_t)} \frac{1+(\gamma-1)/2\ M_i^2}{(1.88M_i-1)M_i} \frac{1.2}{\gamma} \frac{p_a}{p_c} \tag{19}$$

Thus, one obtains

$$\Delta l_{fl} = K_{fl}\ r_t \frac{p_w}{p_c} \frac{1}{\frac{d(p_w/p_c)}{d(1/r_t)}} \frac{1}{1 - \frac{1+(\gamma-1)/2\ M_i^2}{(1.88M_i-1)M_i} \frac{1.2}{\gamma}} \tag{20}$$

The shape of the unsymmetrical separation line is described by the coefficient k_g. For this shape coefficient, which cannot exceed 1, the following values apply:

$K_g = 1$: unsymmetry at 180° of the nozzle circumference (maximum side load)
$= \frac{\pi}{4}$: inclined separation plane
$= 0.3\text{-}0.4$: effective value [15]
$= 0$: symmetrical separation line

According to the simplified side load equation (4), one can write:

$$F_{sl} = 2\ r\ K_g\ \Delta l_{fl}\ p_a\ (1 - \frac{p_i}{p_a}) \tag{21}$$

In this case, r is the average nozzle radius at the point at which the side load impacts. If one used (2) in (21), then it becomes:

$$F_{sl} = 2\, K_g\, K_{fl}\, \frac{r}{r_t}\, r_t^2\, \frac{p_i}{p_a}\, \frac{p_a}{p_c}\, p_a\, \left(1 - \frac{p_i}{p_a}\right) \cdot \cdot \frac{1}{\frac{d(p_w/p_c)}{d(1/r_t)}} \cdot \frac{1}{1 - \frac{1+(\gamma-1)/2\, M_i^2}{(1.88 M_i - 1) M_i}\, \frac{1.2}{\gamma}} \tag{22}$$

The maximum side load occurs if the separation point is distanced from the nozzle end by about the distance Δl_{fl} according to equation (13). With normal nozzles (with a constant pressure fall on the wall along the axis) it corresponds to a pressure ratio which is about 10-20% below that of the full flowing nozzle. This value should be used in (22). /38

At higher pressure ratios p_c/p_a the side load decreases almost linearly until it nearly disappears with a fully flowing nozzle.

The side load equation (22) yields a small side load maximum with low pressure ratio as is also observed in the experiment. In any case, the quantitative ratios are not reflected, probably because with bell nozzles the separated jet in the vicinity of the throat occurs again lower on the wall.

According to (22) with the throat measurements (thrust) and the local surface ratio, the side loads increase. The smaller the oscillations and the flow unsymmetry are (cold gas model), the smaller the side loads become. The most important influence on the intensity of the side load is the nozzle wall pressure gradient. With increasing pressure gradients, the side loads decrease (Table 4); low pressure gradients lead to high loads (J-2D, Atlas sustainer). High pressure ratios in the nozzle (high pressure engine) also yield low side loads.

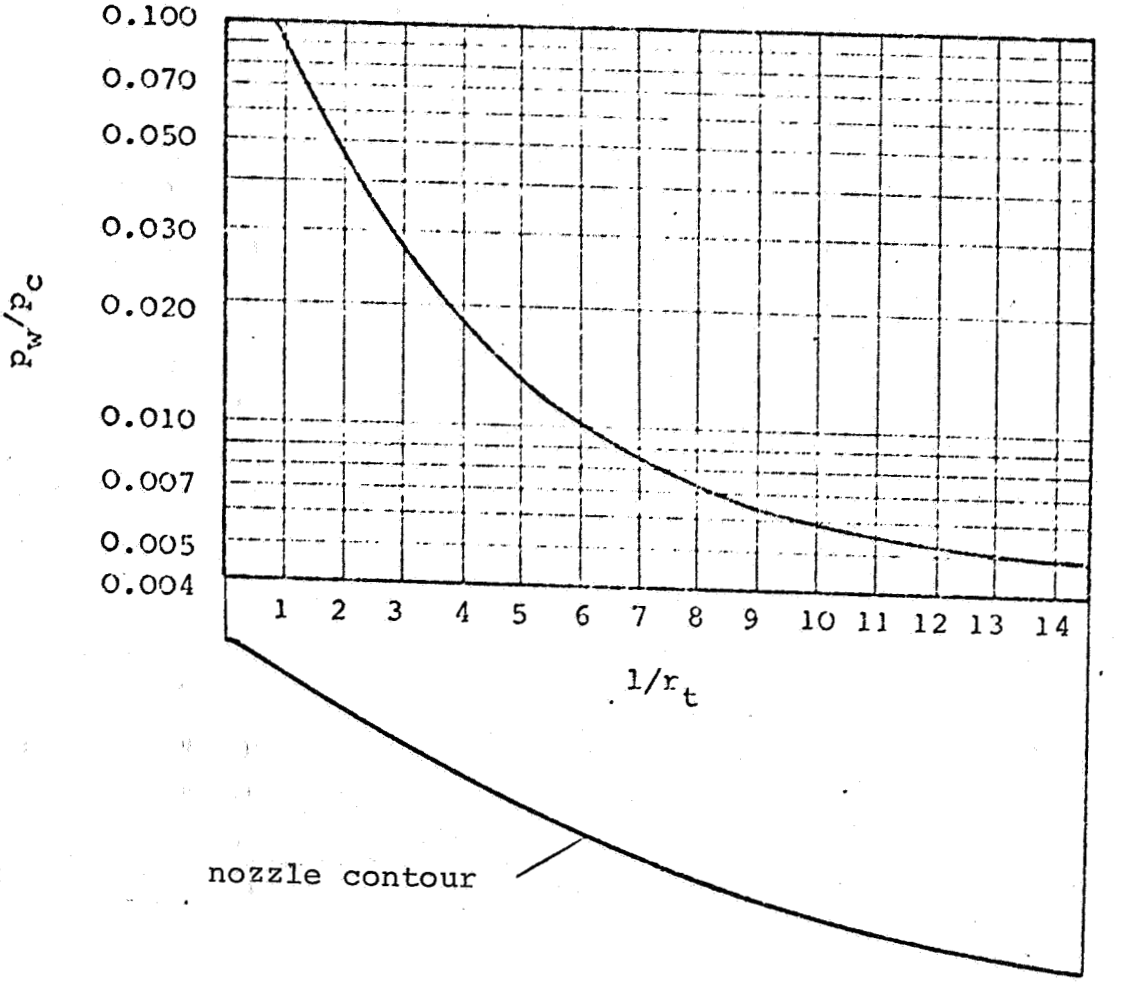

Figure 21. Nozzle contour and wall pressure distribution of the J-2S engine [6,14].

With the help of equation (22), the side loads of a known engine can be converted to a new similar engine. If one assumes that p_i, k_{fl} and k_g are nearly the same, then from (22) there are some simplifications.

$$F_{sl} = F_{sl_{te}} \left(\frac{r_t}{r_{t_{te}}}\right)^2 \left(\frac{\varepsilon}{\varepsilon_{te}}\right)^{0.5} \frac{p_{c_{te}}}{p_c} \left.\frac{\frac{d(p_w/p_c)}{d(1/r_t)}}{\frac{d(p_w/p_c)}{d(1/r_t)}}\right|_{te} \qquad (23)$$

In (23), the index te designates the available test values, ε describes the local opening ratio.

3.2.3 Use of side load model

3.2.3.1 J-2S engine

The only reliable side load measurements are from the J-2S. It is, therefore, useful to test the side load theory qualitatively and quantitatively with the experimental data.

The contour and the wall pressure distribution of the J-2S nozzle are shown in Figure 21. For the computation of the side load, the coefficient k_{fl} as a function of the pressure ratio must be known.

A possibility for this is the evaluation of non-stationary wall pressure measurements as are shown in Figures 17 and 18. Figure 22 shows the oscillation times during the start phase of the J-2D engine (NASA-MSFC S-OVB Test Series) and the resulting oscillation widths. If these measurement results are evaluated, then the average value is /40

$$K_{fl} = 0.05 \ (\pm 20\%)$$

(With a more exact determination of k_{fl}, for which in any case considerably more data must be available, it should be considered that K_{fl} must be constant. The fluctuation coefficient can depend on

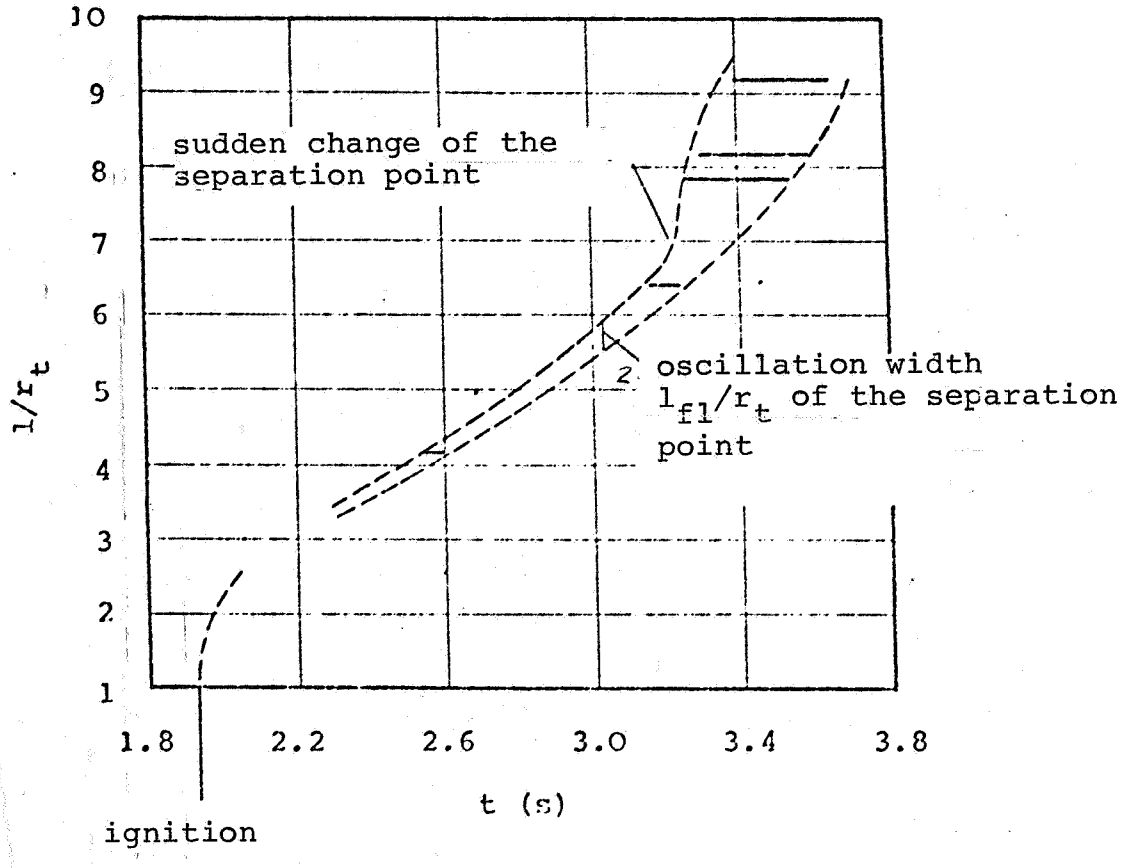

Figure 22. Pattern of the separation point during the starting phase of the J-2D engine and the resulting oscillation width (NASA-MSFC J-2 S-IVB Test Series)

———oscillation period of the measurement point

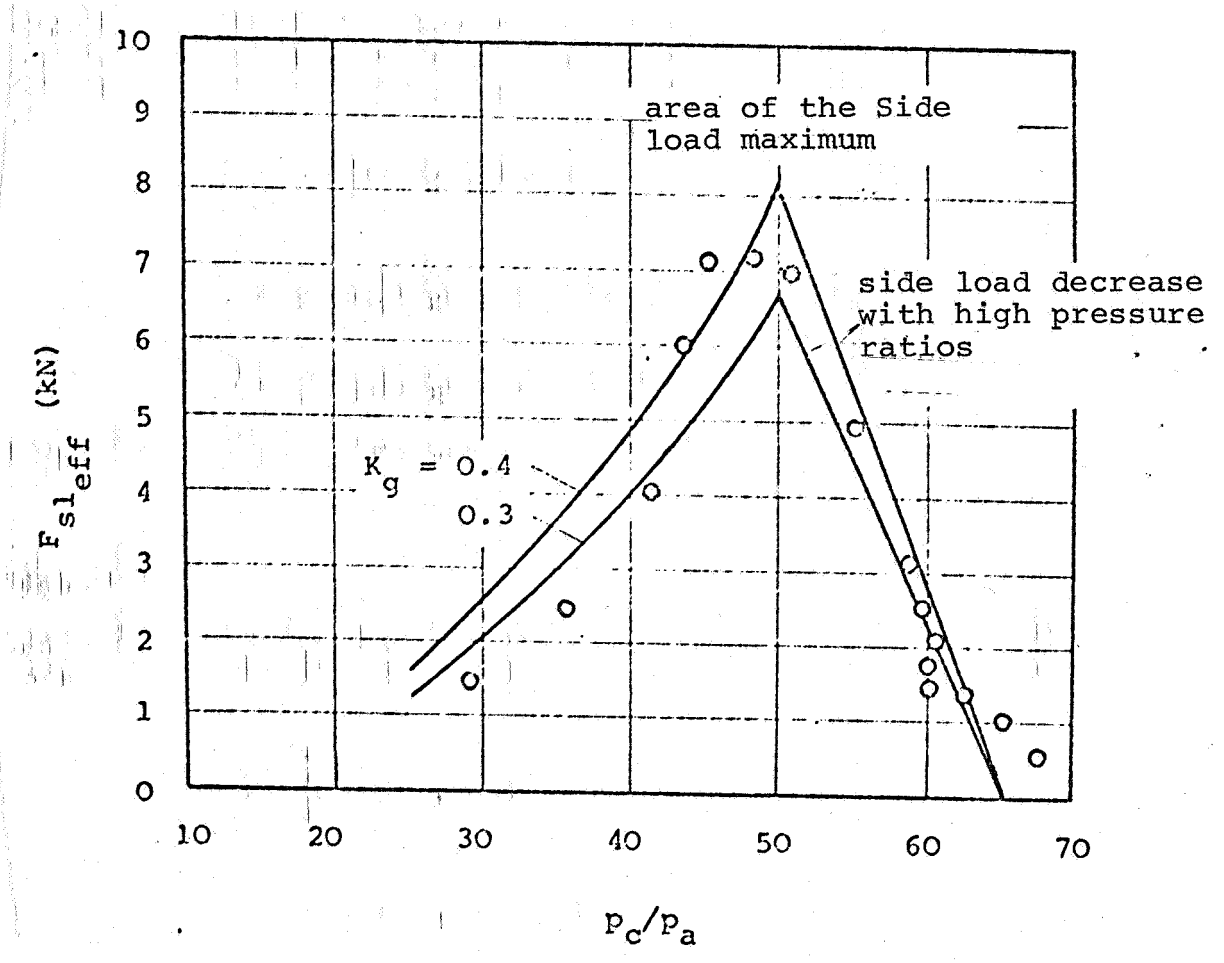

Figure 23. Comparison between experimental and computed effective side loads of the J-2S engine

parameters, such as Mach number. With liquid engines, the coupling between the conveyor system and the injection head can also play a part since with pressure ratios below the design point the stability of the operation can be reduced (pressure oscillations in the Atlas sustainer engine from about 4 bar during the starting phase [7]). The above number can, however, be used as a standard value for these types of engines.

Since only effective values are avilable for side load data 0.3 to 0.4 are used for K_g. The side loads computed with these values as a function of the pressure ratio are shown in Figure 23. It indicates that the computation and measurement values agree rather well.

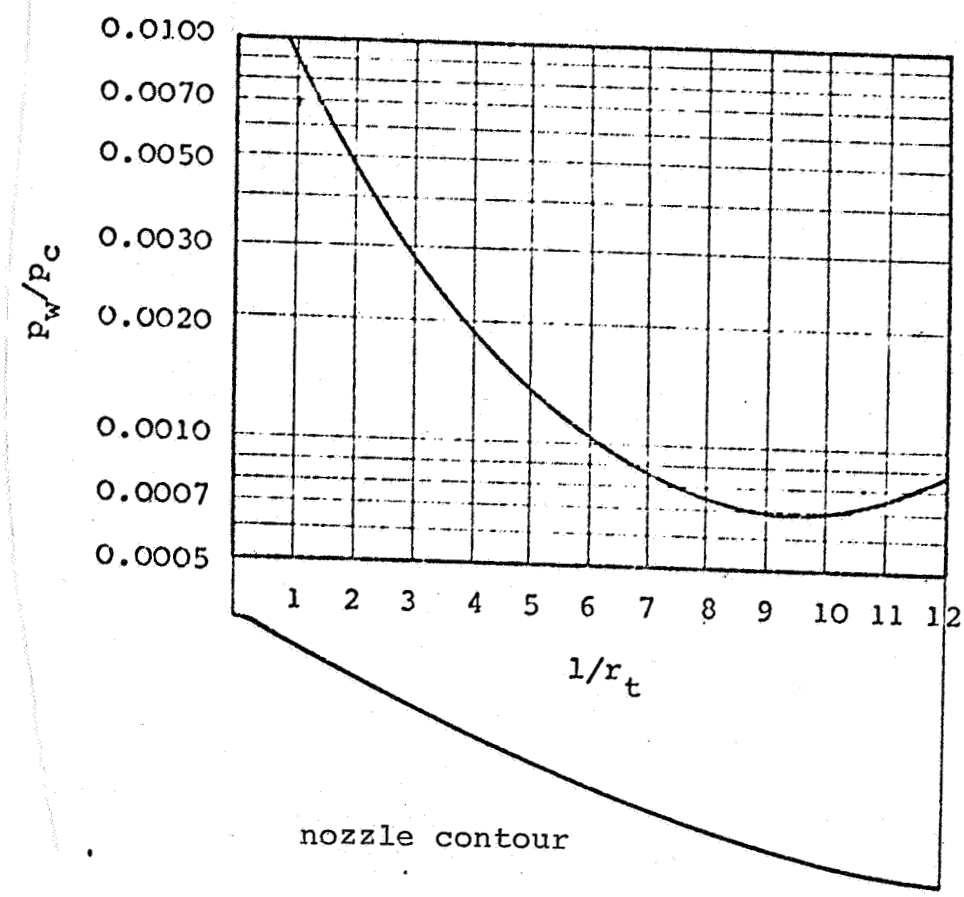

Figure 24. Nozzle contour and wall pressure distribution of the J-2D engine 18

The dispersion is caused by the errors in side load measurements as well as by the simplifications in the determining of the constants. With these values the side loads of a new rocket engine can also be computed.

3.2.3.2 J-2D engine

The J-2D engine is characterized by especially high side loads. The nozzle contour and the wall pressure distribution of this rocket engine are shown in Figure 24.

This nozzle contour differs from the usual nozzle types in that the wall pressure increases over a wide area of the nozzle

length in spite of a nozzle expansion. This pressure increase leads to two (stable) separation points in one part of the nozzle with separation of the flow. Model tests show that in the area of minimum wall pressure the position of the separation point /43
can alter rapidly as a function of the pressure ratio. The pattern of the separation point during the starting phase in Figure 22 shows that the oscillation widths expand suddenly in this zone. If this sudden change is not rotation-symmetrical, then side loads result.

The side loads of this nozzle configuration increase with increasing combustion chamber pressure almost in the usual manner. If the unsymmetry of the nozzle flow and the fluctuations reach the area of the two possible separation points, then the side loads increase rapidly. Figure 1 shows this pattern. The measurements yield a pressure ratio p_c/p_a of 39 for the side load maximum (after the rapid side load increase the side loads decrease with increased pressure ratio), and the computations show a value of 38. Thus, theory and experiment agree quite well. A quantitative comparison of the side load values is not possible since the measurement data of the J-2D engine are increased by the dynamics of the machine oscillations.

The rapid change in the separation point is primarily caused by the unsymmetries in the release of the gases in the nozzle. Through this the loads are almost stationary. Figure 25 shows the time elapse of the operating cylinder and support load through side loads of the J-2D and the J-2S engines. With the J-2S engine, the quasi-stationary portion is very small since the nozzle shows a continual pressure decrease and almost only oscillations of the separation point occur. With the J-2D engine primarily quasi-stationary, loads are observed which are caused by rapid position change of the separation point. The various frequencies result from the different types of suspensions.

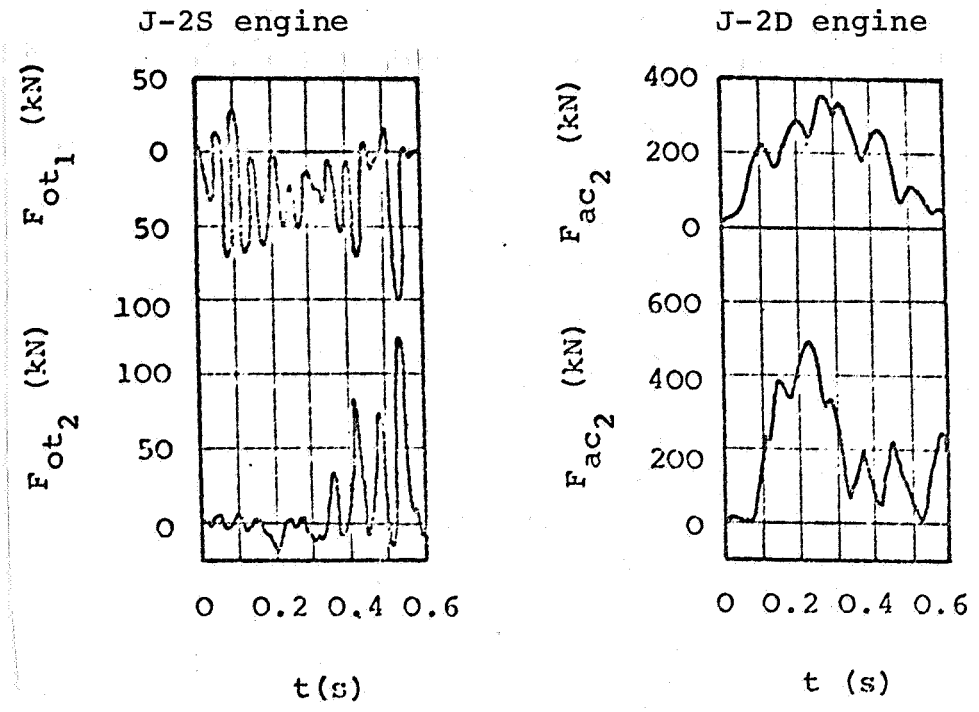

Figure 25. Time elapse of the side loads with the J-2D and J-2S engine during the starting phase [14,16].

F_{ac} operating cylinder load
F_{ot} load of the side support

3.2.3.3 Self-generation of side loads

An important question in the cause of side loads is the question concerning the possibility of the self-generation of side loads.

A bending of the nozzle (see paragraph 2.2.2) alters the wall pressure distribution and the pressure gradients. According to term (22) the side load is influenced by this. Due to the experimentally determined large fluctuation range, this pressure change has only a little influence on the side load so that the effect of the self-generation makes no difference. The J-2S measurements in which the rigidity of the suspension was altered in order to be able to determine an influence of the self-generation

confirm this theoretical result. Therefore, the minor effect of the self-generation can be disregarded concerning the causes of side loads.

REFERENCES

[1] Aerojet Liquid Rocket Company: Nozzle Side Loads Study, Space Shuttle Main Engine Definition Study, Phase B. ALRC, Contract NAS8-26188 (Sept. 11, 1970)

[2] Aerojet Liquid Rocket Company: Actuator Leads Generated by Unsteady Nozzle Gasdynamic Forces during Engine Start (Sea Level Conditions). Contract NAS8-26188. Letter to R. Rodgers, NASA-MSFC, S&E-ASTN-E, from L. A. Holcomb (Feb. 24, 1971)

[3] Barrere, M. and Associates: Rocket Propulsion. Elsevier Publishing Company, New York, 1961

[4] Buschulte, W., K. Schadow: Consideration of Arbitrary Cross Thrust Components in Solid Fuel Engines DLR-FB 1965-06 (1965)

[5] Fenwick, J., M. Moriarty, L. Nave, A. Petersen: Test Results and Analyses of J-2S Engine Side Load Program. Rocketdyne Division, NAR, Report CDR 3124-4087 (April 27, 1973)

[6] Fuller, P. N.: J-2S Nozzle Side Load Study, Final Report. Rocketdyne Division, NAR, Report R-9045 (Aug. 1, 1972)

[7] Hege, D. W.: Semi-Annual Technical Program Report, Atlas. Rocketdyne Division, NAA, Report R-345-1P (AFO4(645)-1) (Dec. 30, 1956)

[8] Kistler, A. L.: Fluctuating Wall Pressure under a Separated Supersonic Flow. Journal of the Acoustical Society of America, Vol. 36, No. 3 (March 1964) pages 543-550.

[9] Kuehn, D. M.: Experimental Investigation of the Pressure Rise Required for the Incipient Separation of Turbulent Boundary Layers in Two Dimensional Supersonic Flow. NASA Memo 1-21-59A (1959)

[10] Lawrence, R. A.: Symmetrical and Unsymmetrical Flow Separation in Supersonic Nozzles. Southern Methodist University, Dallas, Texas, Ph. D. Thesis 1967

[11] Pratt & Whitney Aircraft: Nozzle Separation Data for MSFC. P&WA Florida Research and Development Center. Letter to E. A. Lehmann from F. W. MacAbee, Jr. (Sept. 19, 1969)

[12] Pratt & Whitney Aircraft: Space Shuttle Main Engine Definition (Phase B), Engine Side Loads. P&WA-FR-4468 (April 21, 1971)

[13] Rocketdyne Analysis of Predicted Side Loads in the Nozzles of the Space Shuttle Booster and Orbiter Main Nozzles. Rocketdyne Division, NAR, Report SSE 4.1.1D-1414-2 (August 31, 1970) /46

[14] Rocketdyne: SSME Program: Engine Side Load Study. Rocketdyne Division, NAR, SSME Phase CD Proposal Package (RSS-8502-3) (May 25, 1971)

[15] Rocketdyne: Interface Control Document Items. Letter to L. O. Wear, NASA-MSFC, PM-EP-EM (72 RC 7028) (Sept. 29, 1972)

[16] Rocketdyne: unpublished separation data

[17] Schmucker, R. H.: Side Loads in Liquid Rocket Engines. in: 1st Annual MSFC-Research and Technology Review. George C. Marshall Space Flight Center (Feb. 22, 1973)

[18] Schmucker, R. H.: Flow Processes in the Operation of Overexpanded Nozzles of Chemical Rocket Engines. Part 1: Flow Separation. Technological University Munich, Faculty for Space Technology, Report TB-7 (July 3, 1973)

[19] Thayer, E. B., D. E. Booz: Flow Separation Tests of Candidate Space Shuttle Nozzles. Pratt & Whitney Aircraft FR-SMR-3491 (Nov. 21, 1969)

[20] Tuovila, W. J., N. S. Land. Experimental Study of Aeroelastic Instability of Overexpanded Rocket Nozzle Extensions. NASA TN D-4471 (April 1968).

APPENDIX A: Listing of important side load models /A1

1. Pratt & Whitney Aircraft Side Load Model

The side load model of Pratt & Whitney Aircraft is essentially based on the experimental studies of Lawrence [10], which were carried out with small cold gas nozzles and which permit the computation of side load of a new but similar engine with knowledge of various constants which must be determined in the test.

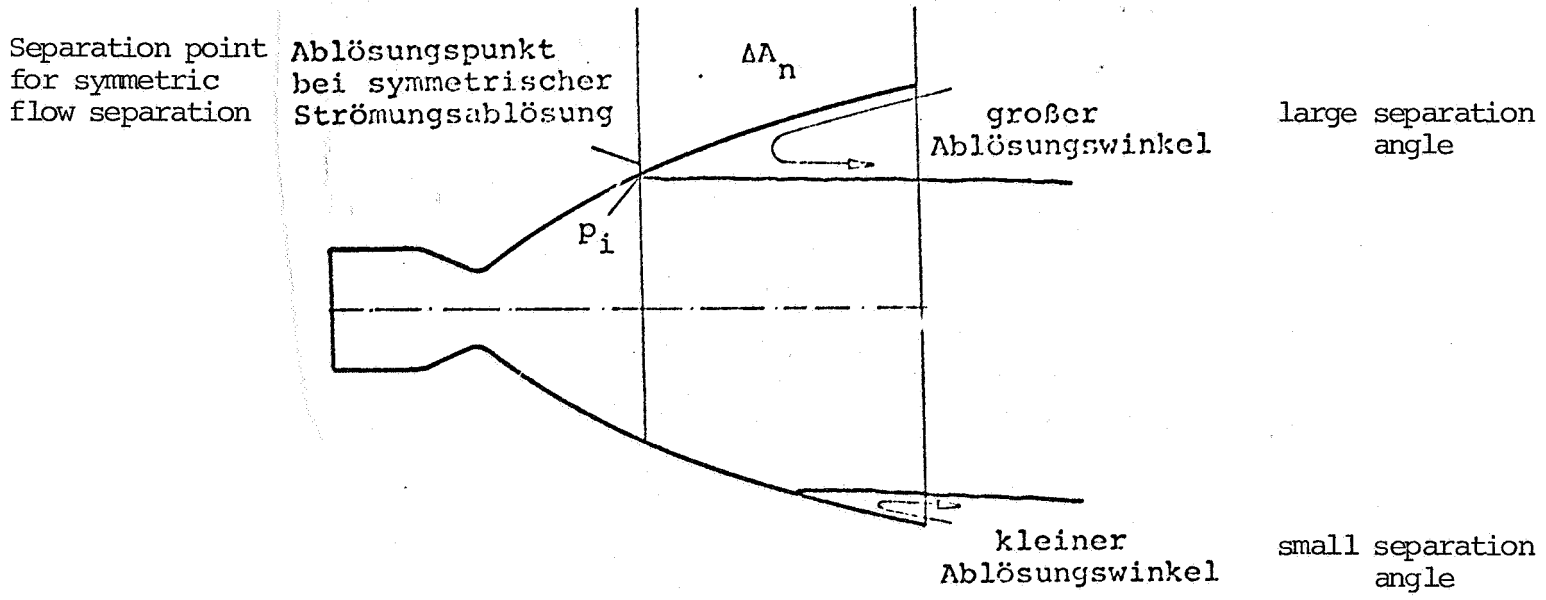

Figure A1. Side load model, Pratt & Whitney Aircraft

Figure A1 is the mechanism which the side load generation is based on. With bell-shaped nozzles, the flow separation occurs far upwards and, therefore, the separation line is rather symmetrical due to the high angle of divergence. In the area around the nozzle end the angle of divergence is very small and the back flow of the environmental air occurs unsymmetrically since the error in the circumferential direction cannot be equalized. Through this an unsymmetrical separation line occurs.

The empirical equation for the side load depends on two parameters, the combustion chamber pressure at which the nozzle flows fully, $p_{c_{ff}}$, and the projected nozzle surface between the separation point with symmetrical flow separation and the nozzle end ΔA_n. If the index te designates the known test values with maximum side load, then the side load equation is written: /A2

$$F_{sl} = F_{sl_{te}} \frac{p_{c_{ff}}}{p_{c_{ff_{te}}}} \frac{\Delta A_n}{\Delta A_{n_{te}}} \tag{A1}$$

The combustion chamber pressure at which the nozzle flows fully is obtained from the vacuum wall pressure at the nozzle end p_e and the environmental pressure from Schilling's separation criterion [18] as

$$p_{c_{ff}} = 0.0635\ p_a \left(\frac{p_e}{p_a}\right)^{-5.12} \tag{A2}$$

The maximum side loads occur at combustion chamber pressure $p_{c_{sl}}$. This pressure depends on the combustion chamber pressure $p_{c_{ff}}$, and the ratio of both pressures is accepted as constant at $k_{c_{sl}}$. Thus, for the wall pressure p_i, up until the maximum side load that symmetrically flows through the nozzle, according to (A2) one gets:

$$p_i = 0.583\ p_a \left(\frac{p_{c_{ff}}\ K_{csl}}{p_a}\right)^{-0.195} \tag{A3}$$

where

$$K_{csl} = \frac{p_{c_{sl}}}{p_{c_{ff}}} \tag{A4}$$

The projected areas can then be obtained from the wall pressure distribution and the geometric measurements of the nozzle.

The test values, which were necessary in the equation (A1), /A3
stem from a 1130 kN (250 k) LOX/LH_2 high drag engine. During the final phase of combustion, the nozzle oscillates as a result of the side loads. The evaluation of film exposures permits the determination of the maximum nozzle deflection and the combustion chamber pressure at which this deflection occurs. From this movement, if the force assault point is established, the side load is determined. For the test values the following is used:

$$\frac{F_{sl_{te}}}{p_{c_{ff_{te}}} A_n} = 0.00717 \qquad \text{(A5)}$$

and

$$K_{csl} = 0.271 \qquad \text{(A6)}$$

2. Aerojet Liquid Rocket Company side load model

The side load model from Aerojet is shown in Figure A2. Like Pratt & Whitney Aircraft, it also used the experiments of Lawrence [10] and supplements his observations with data from /A4
Rocketdyne which are listed in [18].

The cause of the side loads is normal flow separation on one side of the nozzle and reapplication of the flow on the remaining part. Since with separation and reapplication the wall pressure can fall to lower values than with pure separation before the recompression occurs on the external pressure, an unsymmetrically separated area develops which produces the side loads. The computation of the separation pressures is based on the Arens-Speigler model in the case of the pure separation which is shown in [18]. In the determination of the separation pressure inclined separation, isentropic back compression in the recirculation zone, back-up in the reflected compression shock according to the Arens-Spiegler model, and expansion with constant pressure ratio are assumed for separation and reapplication. The resulting separation pressures

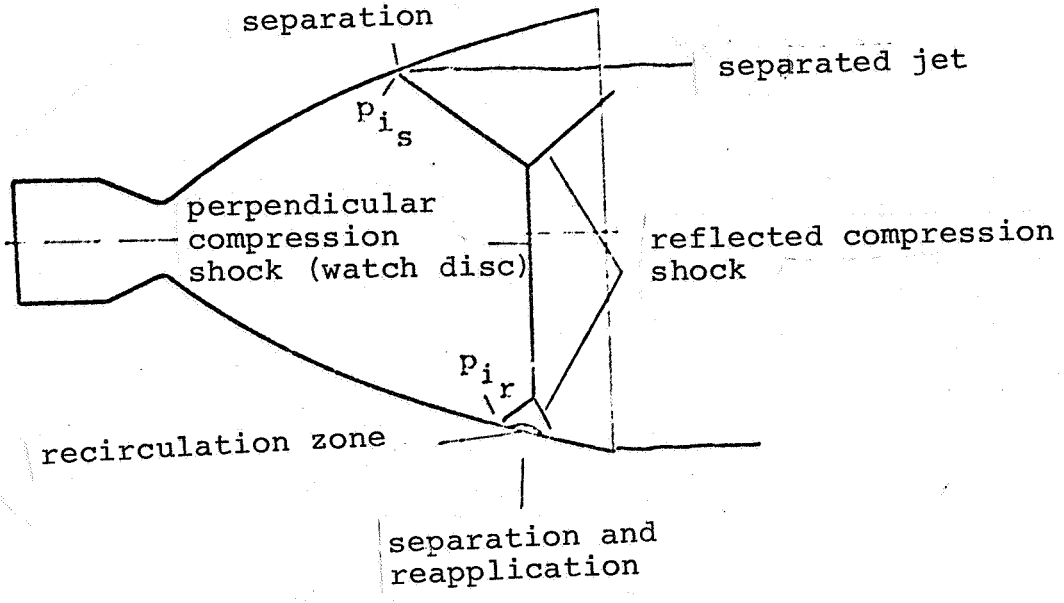

Figure A2. Side load model from Aerojet

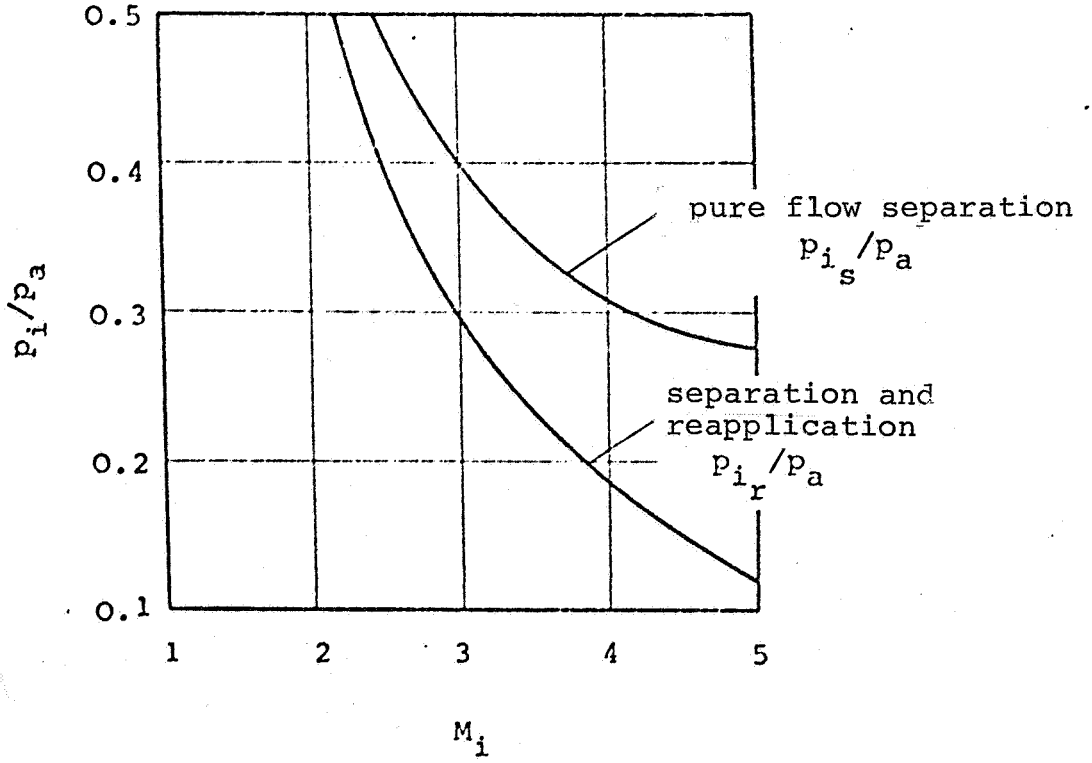

Figure A3. Separation pressures with pure flow separation and separation and reapplication above Mach number M_i at the separation point ($\gamma = 1.4$).

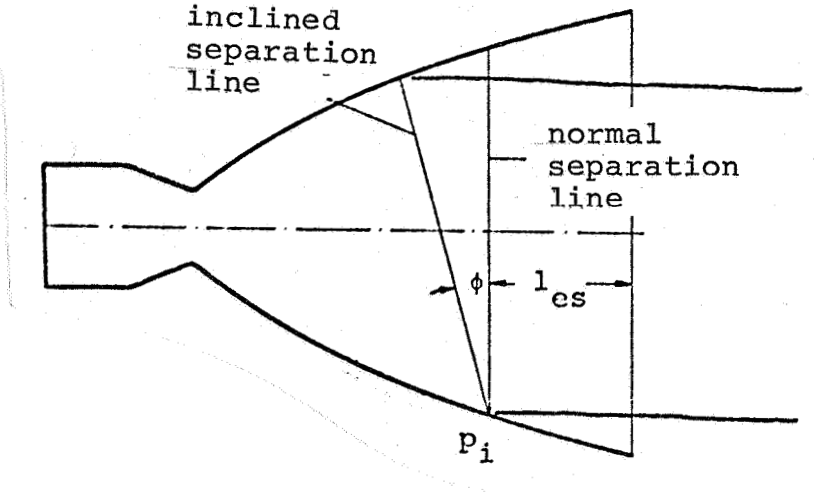

Figure A4. Side load model of Rocketdyne

are shown in Figure A3. The curves represent an isentropic exponent of 1.4 since this value agrees best with the experimentally flow separation data used.

The maximum side load occurs if one-half of nozzle separates /A5 normally and the flow is again directed at the other. With the wall pressure distribution and the geometry of the nozzle, the side load pattern can be computed for variable combustion chamber pressure using the separation pressures of Figure A3 and thus determines the maximum side load and the applicable chamber pressure.

3. Rocketdyne side load model [13,14,15]

The side load model of Rocketdyne is based on an empirical correlation in order to compute the size of the unsymmetrically separated area in the nozzle. With the knowledge of the various mathematical inter-relationships which must be determined in the test, the computation of the side load of a new but similar engine is possible.

This model is depicted in Figure A4. The flow separation takes place along a plane inclined toward the nozzle axis.

The wall pressure at which the symmetrical separation (normal separation line) occurs is determined according to the criteria of Donaldson-Lange as shown in [18]+. With this the distance of /A6
the separation line from the nozzle end l_{se} is obtained. With the predominant geometrical measurements at this nozzle point, an angle ϕ can be determined with which the side load developing at this combustion chamber pressure is produced. The correlation for the inclination of the separation line has the following general form:

$$\phi = \phi(p_i/p_a,\ l_{sc}) \qquad \text{(A7)}$$

whereby

$$l_{se} = l_{se}(p_i/p_a,\ p_w)$$

With the new engine the separation point is determined according to the separation pressure ratio p_i/p_a and the theoretical wall pressure. The correlation for the angle and the local nozzle diameter leads to the side load via the wall pressure.

(Through a modification of this process--instead of the angle of the inclined separation plane the boundary pressures with the unsymmetrical separation are determined--a side load prediction can be obtained which corresponds to that of equation (22)).

The data is based on the measurement values of the J-2 /B2
engine from paragraph 3.2.3. The value of the side load maximum and the applicable pressure ratio deviates only insignificantly from the prediction of Rocketdyne.

+In [13,14] $p_i/p_a = 0.285$ is assumed as separation pressure.

APPENDIX B: Side load predictions for the space shuttle main engine. /B1

The effective side load for the nozzle configuration shown in [18] for the space shuttle main engine is shown in Figure B1.

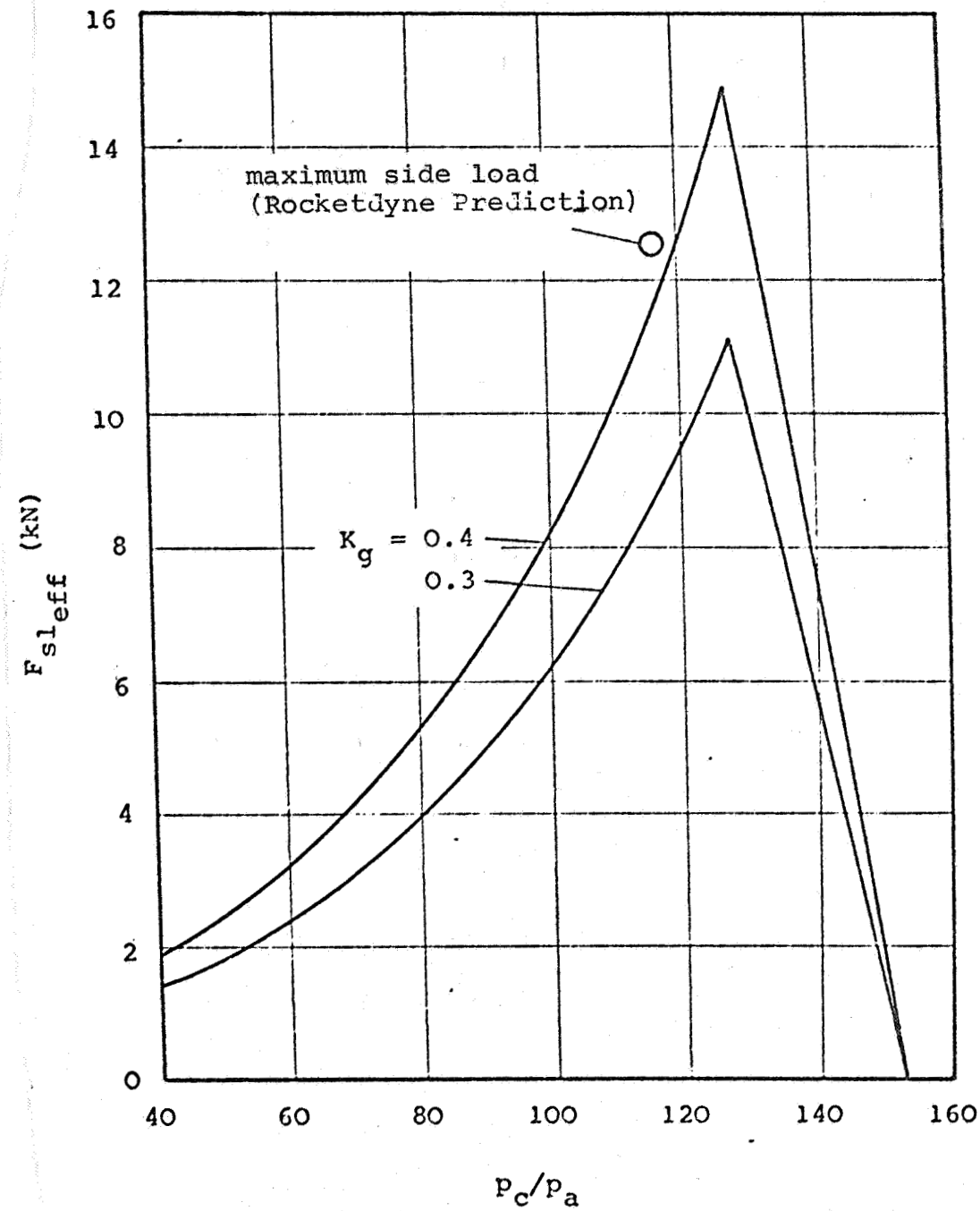

Figure B1. Side load prediction for the space shuttle main engine.